

1  
2  
3  
4  
5  
6  
7  
8  
9  
10  
11  
12  
13  
14

# JMB

Available online at www.sciencedirect.com

SCIENCE @ DIRECT®



15  
16  
17  
18  
19  
20  
21  
22  
23  
24  
25  
26  
27  
28  
29  
30  
31  
32  
33  
34  
35  
36  
37  
38  
39  
40  
41  
42  
43  
44

## Binding of the Respiratory Chain Inhibitor Antimycin to the Mitochondrial *bc*<sub>1</sub> Complex: A New Crystal Structure Reveals an Altered Intramolecular Hydrogen-Bonding Pattern

45  
46  
47  
48  
49  
50  
51  
52  
53  
54  
55  
56  
57  
58  
59  
60  
61  
62  
63

Li-shar Huang, David Cobessi, Eric Y. Tung and Edward A. Berry\*

Physical Biosciences Division  
Lawrence Berkeley National  
Laboratory, 1 Cyclotron Road  
Berkeley, CA 94720, USA

Antimycin A (antimycin), one of the first known and most potent inhibitors of the mitochondrial respiratory chain, binds to the quinone reduction site of the cytochrome *bc*<sub>1</sub> complex. Structure–activity relationship studies have shown that the *N*-formylamino-salicyl-amide group is responsible for most of the binding specificity, and suggested that a low *pK*<sub>a</sub> for the phenolic OH group and an intramolecular H-bond between that OH and the carbonyl O of the salicylamide linkage are important.

Two previous X-ray structures of antimycin bound to vertebrate *bc*<sub>1</sub> complex gave conflicting results. A new structure reported here of the bovine mitochondrial *bc*<sub>1</sub> complex at 2.28 Å resolution with antimycin bound, allows us for the first time to reliably describe the binding of antimycin and shows that the intramolecular hydrogen bond described in solution and in the small-molecule structure is replaced by one involving the NH rather than carbonyl O of the amide linkage, with rotation of the amide group relative to the aromatic ring. The phenolic OH and formylamino N form H-bonds with conserved Asp228 of cytochrome *b*, and the formylamino O H-bonds *via* a water molecule to Lys227. A strong density, the right size and shape for a diatomic molecule is found between the other side of the dilactone ring and the  $\alpha$ A helix.

© 2005 Published by Elsevier Ltd.

**Keywords:** cytochrome *bc*<sub>1</sub>; antimycin; respiratory chain; membrane protein complex; inhibitor binding site

\*Corresponding author

### Introduction

The cytochrome *bc*<sub>1</sub> complex is an enzyme (E.C. 1.10.2.2, ubiquinol:cytochrome *c* oxido-reductase) that comprises the middle part of the mitochondrial respiratory chain. It is a multi-subunit membrane

protein, with ten or 11 protein chains in mitochondrial forms and three or more in bacterial complexes. It always contains the three redox subunits cytochrome *b*, cytochrome *c*<sub>1</sub>, and the iron–sulfur protein (ISP); which contain respectively two hemes B, heme C and a Rieske-type Fe<sub>2</sub>S<sub>2</sub>

Present address: D. Cobessi, Ecole Supérieure de Biotechnologie de Strasbourg, UPR9050 CNRS, Boulevard Sebastien Brant, BP 10413, 67412 Illkirch, France.

Abbreviations used: antimycin, antimycin A; cytochrome *bc*<sub>1</sub>, cytochrome *bc*<sub>1</sub> complex; DM, dodecyl maltoside; UDM, undecyl maltoside; HG,  $\beta$ -hexyl-D-glucopyranoside; FSA, formylaminosalicylate moiety of antimycin; CC, correlation coefficient; PDB, Protein Data Bank;  $2F_o - F_c$  map, a map from Fourier coefficients calculated as twice the measured amplitude minus amplitude calculated from the structure and phases calculated from the structure. “N-side” and “P-side” refer to the normally negative matrix side and positive inter-membrane side of the inner mitochondrial membrane. Structures that have been deposited in the PDB are referred to by their capitalized 4-character accession codes (e.g. “1P84”). Their authors and literature references can be obtained from the entry at the PDB if not given here. heme *b*<sub>H</sub> and heme *b*<sub>L</sub> refer to the high and low-potential hemes of cytochrome *b*. Heme B refers to Fe-protoporphyrin 9 irrespective of oxidation state. Heme C refers to a modified Heme B in which both vinyl groups of the porphyrin have been saturated by addition of cysteine S<sup>γ</sup> forming covalent links to the protein.

E-mail address of the corresponding author: eaberry@lbl.gov

127 iron-sulfur cluster. It catalyzes reversible electron  
128 transfer from ubiquinol to cytochrome  $c$  coupled to  
129 proton translocation across the inner mitochondrial  
130 membrane, probably by a mechanism like the  
131 "protonmotive Q cycle".<sup>1-4</sup>

132 The existence of inhibitors specifically binding to  
133 and inhibiting the two ubiquinone reaction sites  
134 was critical in the elucidation of the Q-cycle  
135 mechanism. One of the earliest known (for a review  
136 of early work see Slater<sup>5</sup>) and most potent (with a  
137  $K_D$  on the order of 30 pM<sup>5</sup>) of these is antimycin A  
138 (antimycin). Antimycin binds specifically to the  
139 quinone reduction site ( $Q_i$  site) of the cytochrome  
140  $bc_1$  complex. When bound, the UV-visible spectrum  
141 of the high-potential cytochrome  $b$  is shifted to the  
142 red and the fluorescence of antimycin is quenched,  
143 leading to the conclusion<sup>6</sup> that antimycin binds near  
144 the heme  $b_H$ .

145 Together with British Anti-Lewisite (BAL) or  
146 alkyl-hydroxynaphthoquinone (HNQ), antimycin  
147 enabled the demonstration of two independent  
148 pathways for reduction of cytochrome  $b$  by  
149 ubiquinol, one sensitive to antimycin and the  
150 other blocked by BAL treatment or HNQ, in the  
151 "double-kill" experiment.<sup>7</sup>

152 When antimycin is bound, the  $bc_1$  complex  
153 exhibits an unexpected inverse relation between  
154 the redox poise of the high potential chain (iron-  
155 sulfur protein and cytochrome  $c_1$ ) and that of the  $b$   
156 cytochromes, resulting in phenomena coined  
157 "oxidant-induced"<sup>8</sup> and "reductant-controlled"<sup>9</sup>  
158 reduction of  $b$  cytochromes. This is explained in  
159 the Q-cycle mechanism (Scheme 1) and in an earlier  
160 model<sup>10</sup> by having the  $b$  cytochromes and the high-  
161 potential chain connected to each of two sequential  
162 one-electron steps in the oxidation of quinol at the  
163 antimycin insensitive ( $Q_o$ ) site. In the Q-cycle  
164 scheme antimycin blocks the reaction at the  $Q_i$   
165 site, at which cytochrome  $b$  equilibrates directly  
166 with the ubiquinone/ubiquinol couple, masking  
167 the oxidant-induced reduction in the absence of  
168 antimycin.

169 Generation of a semiquinone at the  $Q_i$  site is  
170 expected from the Q-cycle mechanism due to  
171 sequential one-electron reduction of quinone there  
172 by successive turnovers of the  $Q_o$ -site reaction.  
173 A semiquinone signal has been observed by EPR  
174 spectroscopy and it is eliminated by anti-  
175 mycin,<sup>11,12</sup> consistent with the predictions of  
176 the Q-cycle scheme. Thus antimycin could be  
177 considered a marker for the  $Q_i$  site of the  
178 Q-cycle mechanism.

179 Antimycin dramatically increases the stability of  
180 the bovine  $bc_1$  complex in the presence of bile salt  
181 detergent taurocholate,<sup>13</sup> inhibiting the "cleavage"  
182 reaction quantitatively at stoichiometric concen-  
183 trations. These and other observations<sup>6,14-16</sup> led to  
184 the conclusion that antimycin-binding induces a  
185 far-reaching conformational change in the cyto-  
186 chrome  $bc_1$  complex. Dithionite reduction of the  
187 complex results in a similar protection against  
188 cleavage,<sup>13</sup> and affects the apparent cooperativity  
189 of antimycin binding<sup>6</sup> suggesting that redox state of

190 cytochrome  $b$  may also be coupled to the confor-  
191 mational change. More recent indications of an  
192 antimycin-induced conformational change include  
193 an effect of antimycin on the sensitivity of the iron-  
194 sulfur protein to proteolytic cleavage,<sup>17</sup> and an  
195 apparent effect of antimycin on "half-the sites  
196 reactivity" of the  $Q_o$  site.<sup>18</sup>

197 One model<sup>19</sup> for the reaction mechanism of the  
198  $bc_1$  complex invokes conformational coupling  
199 between events at the  $Q_i$  site, where antimycin  
200 binds, and the  $Q_o$  site, where the bifurcated  
201 transfer of electrons from ubiquinol to cytochrome  
202  $b$  and the iron-sulfur protein must be enforced to  
203 maintain proton-pumping efficiency. After different  
204 positions of the ISP ectodomain were observed in  
205 crystals and proposed to be involved in the catalytic  
206 cycle,<sup>20</sup> it was suggested<sup>21,22</sup> that such confor-  
207 mational coupling might prevent the ISP from  
208 returning to the  $Q_o$  site until the second electron  
209 had passed to heme  $b_H$  and the  $Q_i$  site, ensuring  
210 bifurcation.

211 Despite the circumstantial evidence for a  
212 conformational change involving the  $Q_i$  site, no  
213 significant conformational change in the N-side or  
214 transmembrane domains of cytochrome  $b$  has  
215 been observed in the crystallographic structures.  
216 With the initial chicken  $bc_1$  structures, we  
217 reported<sup>23</sup> an upper limit of 1Å in the absence of  
218 stigmatellin (and 0.5 Å in its presence) for the  
219 maximum difference of  $C^\alpha$  atom positions (residues  
220 2-380) between crystals with and without anti-  
221 mycin. Gao *et al.*<sup>24</sup> reported rmsd 0.33 Å for all but  
222 one of the 378 residues modeled; comparison of  
223 structures 1ntk and 1ntz shows the largest devi-  
224 ations to be 2.2 Å for residue 2 and 1.4 Å for  
225 residue 267.

226 In potentiometric titrations, it has often been  
227 observed that the cytochrome  $b_{662}$  ( $b_{560}$  in bacteria)  
228 species attributed to heme  $b_H$  titrates hetero-  
229 geneously,<sup>25-30</sup> with part showing a midpoint  
230 potential ( $E_m$ ) around 150 mV and the rest around  
231 50 mV (in bacterial chromatophores at pH 7). In the  
232 presence of antimycin only the low potential  
233 component is observed.<sup>30,31</sup> In the presence of  
234 funiculosin there is only one component, with  $E_m$   
235 near that of the high potential component.<sup>30,32</sup> If the  
236 system is poised so that  $b_H$  is reduced partly,  
237 addition of antimycin results in oxidation of  
238 cytochrome  $b$ .<sup>25,26</sup> These phenomena have been  
239 explained as due to the mechanism by which  
240 cytochrome  $b_H$  equilibrates with the Q pool *via* the  
241  $Q_i$  site,<sup>26,27,31,33</sup> or alternatively as due to redox  
242 interaction between the cytochrome  $b$  heme and  
243 quinone species at the  $Q_i$ .<sup>29,30</sup> In which the redox  
244 state of one component affects the midpoint  
245 potential of the other. If the latter explanation is  
246 correct, the possibility that antimycin and funicu-  
247 losin mimic different redox states of ubiquinone at  
248 the  $Q_i$  site seems attractive.

249 Thus, there remains a large body of experi-  
250 mental observation concerning antimycin and  
251 the reaction at the  $Q_i$  site that is not very  
252 well explained at present. In the process of

unraveling the details of the reaction, and in explaining these diverse observations, it would be very helpful to know how antimycin, funiculosin, and ubiquinone bind to the site. In addition, the  $Q_i$  site of fungal and other plant pathogens is an important target for crop protection agents.<sup>34,35</sup> The site is of potential significance in treatment of human disease if species-specific inhibitors can be designed. Thus antimycin has been the subject of numerous structure–activity–relationship studies aimed at understanding the mechanism of the enzyme and at developing powerful new crop protection agents.<sup>16,36–41</sup>

Antimycin (Figure 1(a)) has a headgroup consisting of 3-formylamino salicylate, amidified to a dilactone ring consisting of L-threonine (whose amino group is amidified to the salicylate moiety) and a 2-alkyl, 3,4-dihydroxyvalerate. It is the 4-hydroxy group of the latter, which participates in the dilactone, and the 3-OH is esterified by a branched carboxylic acid (acyl side-chain). There is heterogeneity in the 2-alkyl group (alkyl side-chain) and in the acyl side-chain, which at least in antimycin A1 has recently been shown to consist mainly of 2-methyl butanoate<sup>42</sup> rather than isovalerate (3-methyl butanoate) as deduced earlier.<sup>43,44</sup> High-resolution chromatography has resolved commercial antimycin samples into as many as ten different compounds.<sup>45</sup>

Early structure–activity–relationship studies have led to the conclusions that the *N*-formylamino-salicyl group is responsible for most of the binding specificity, and to the importance of a low  $pK_a$  for the phenolic OH group.<sup>16</sup> The dilactone ring and substituents can be replaced by a long-chain fatty amine with retention of tight ( $\mu$ M) binding and inhibition. More recent studies have examined stereo-specificity of the dilactone<sup>37</sup> and probed with substituents at various positions on the salicylamide group.<sup>38,40</sup> Conclusions of the latter studies include the importance of the phenolic OH and formylamino groups and an intramolecular H-bond between the phenolic OH and the carbonyl O of the amide linkage by which the rest of the molecule is connected to the 3-formylaminosalicylic acid.

Antimycin was instrumental in locating the  $Q_i$  site in the first crystal structure of a  $bc_1$  complex,<sup>46</sup> but no coordinates for antimycin were deposited in the Protein Data Bank (PDB). Since then, two structures have been made available with coordinates for antimycin, PDB entries 3BCC (chicken) and 1NTK (bovine). The low resolution of the former structure made it impossible to discern details required for a rigorous description of antimycin binding. Structure 1NTK was processed at higher resolution (2.6 Å); however, the work presented here shows that, it too has errors in the details of binding.

In this work, we introduce two new crystal structures of the bovine mitochondrial  $bc_1$  complex with stigmatellin at the  $Q_o$  site. PDB entry 1PP9

(2.23 Å) has no  $Q_i$ -site ligand added, while 1PPJ (2.28 Å) was co-crystallized with antimycin. This allows us for the first time to reliably describe the binding mode of antimycin at the level of detail required to begin to understand its diverse effects on the  $bc_1$  complex.

## Results

### Resolution and quality of the structures

The diffraction was somewhat anisotropic, as judged by the “falloff” analysis in the program TRUNCATE and by anisotropic scaling during refinement in CNS which gave a  $B$  tensor with diagonal elements  $-15.3, 0.6, 14.7 \text{ \AA}^2$  for 1PP9 and  $-12.5, 3.8, 8.6 \text{ \AA}^2$  for 1PPJ. The data reduction and refinement programs we used have no provision for an ellipsoidal resolution cutoff, so to avoid losing any useful data in the well-ordered directions we used a resolution cutoff of 2.07 for 1PP9 and 2.0 for 1PPJ in the initial data reduction. In the final refinement for deposition and calculation of refinement statistics (Table 1B), a resolution limit of 2.1 Å was used for both structures. This should not be taken as the resolution of the structure, however, as the data in the outer shells were quite weak. A more objective measure of the resolution of a diffraction dataset<sup>47</sup> is given by the “optical” resolution as calculated by the program SFCHECK.<sup>48</sup> However, the optical resolution is defined differently (how close two features can be and still be resolved by the data, rather than as a  $d_{\min}$  cutoff), so they are not directly comparable. A sparse random survey of structures deposited with data during 2002 showed (E. Tung, unpublished results) that in the range of 1.2–3.0 Å the optical resolution  $R_{\text{opt}}$  was related to reported resolution cutoff  $d_{\min}$  by the expression ( $R_{\text{opt}} = 0.42 + 0.59d_{\min}$ ). The datasets for structures 1PP9 and 1PPJ have optical resolution 1.72 and 1.75. By the above relation this is the type of resolution to be expected from the average structure using a resolution cutoff of 2.23 Å or 2.28 Å.

While this resolution is only marginally higher than the best yeast or bovine  $bc_1$  structures available previously, we think the quality of the structures is significantly higher. This is due to the presence of a dimer in the asymmetric unit, which, for the same solvent content, doubles the number of unique reflections at a given resolution. Because non-crystallographic symmetry was quite good for most of the protein, the use of NCS-restraints resulted in effectively doubling the data/parameters ratio with consequent improvement in the refinement process. In addition, while making the final model we had the benefit of using all the previously deposited structures for comparison and evaluation, which we gratefully acknowledge.

At the current state of refinement (Table 1B) the free- $R$  factor is approximately 0.40 in the shell around 2.1 Å for 1PP9, and below 0.4 at 2.0 Å for 1PPJ, suggesting the datasets actually contain some

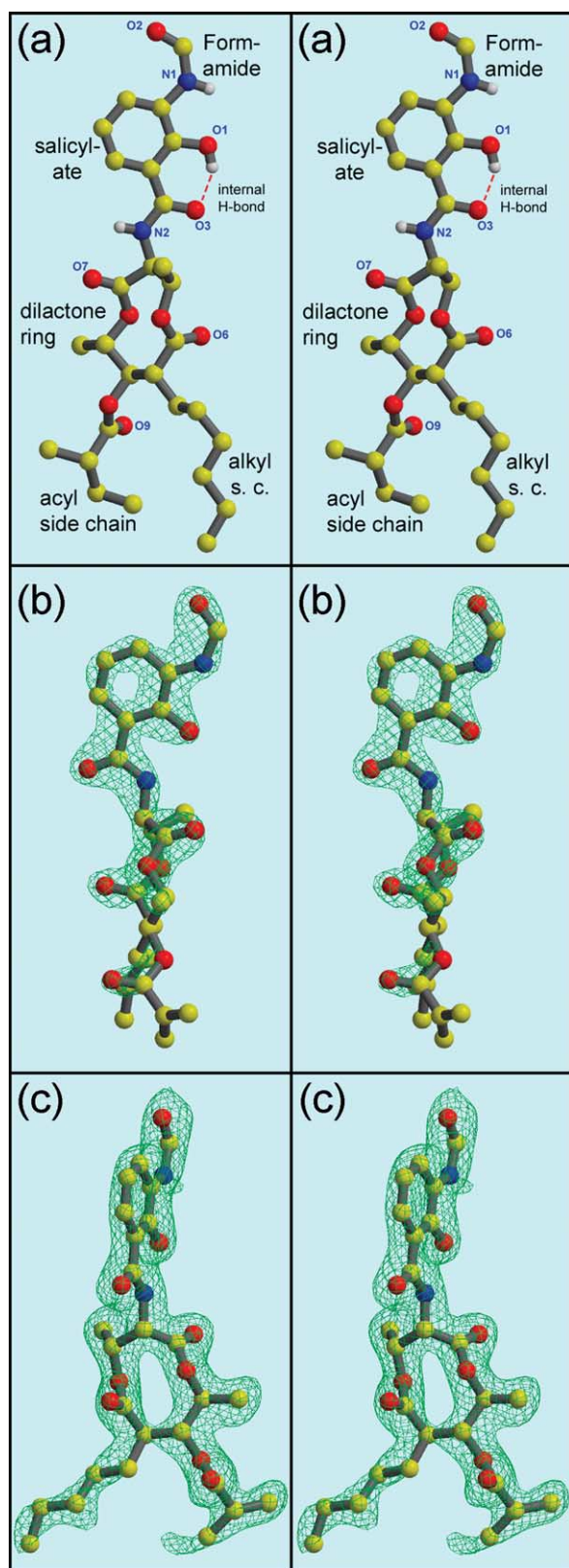


**Figure 1.** The structure of antimycin (stereo views). (a) From the small-molecule crystal structure<sup>42</sup> (coordinates from the Cambridge Structure Database, CCDC # 125007). Hydrogen atoms have been removed from the carbon atoms for clarity. (b) From the structure 1PPJ, with the FSA ring and amide group in the plane of the picture. (c) As (b) but rotated 75° to view the dilactone ring nearly face-on. The electron density in (b) and (c) is a  $2F_o - F_c$  map contoured at  $2.1\sigma$  (b) or  $0.9\sigma$  (c) from structure 1PPJ.

useful information to these resolutions. Analysis of the structures<sup>†</sup> by PROCHECK<sup>49,50</sup> show them to be within the norm or better on all measures as compared to 2.0 Å structures. These structures are the first cytochrome *bc*<sub>1</sub> structures to achieve greater than 90% of the residues in the allowed regions (A, B, L) of the Ramachandran plot, as expected for real proteins based on analysis of structures solved at better than 2 Å with *R*-factors below 20%.<sup>50</sup> Overall real-space *R*-factors are 0.155 and 0.148, and real-space correlation coefficients are 0.909 and 0.921 for structures 1PP9 and 1PPJ, respectively (EDS website<sup>‡</sup>). Representative electron density from well-ordered regions in crystal 1PPJ are shown in stereo pairs of Figure 2 as well as in the figures documenting the mode of antimycin binding (Figures 1, 5, and 6).

Still, the current structures are disordered in a few sections, and so for some features it will be best to look at structures from other crystal forms. In such areas where the structure is not completely determined by the data, the electron density has been interpreted liberally to provide our best guess of the actual arrangement. To avoid over-interpretation of the structure and possible erroneous conclusions concerning features not described in the text, it is important to compare all the available structures, and to examine the electron density on which the feature is based. To facilitate independent evaluation of structural features by others, the original data (structure factor amplitudes) for the structures have been deposited with the Protein Data Bank.

### Overall structure

The overall structure of the eukaryotic *bc*<sub>1</sub> complex has been described.<sup>20,46,51,52</sup> The trans-membrane region is made up of 26 trans-membrane helices, with each monomer contributing 13: eight from cytochrome *b* and one each from subunits 7, 10 and 11 plus the trans-membrane anchor helices of the ISP and

<sup>†</sup> A collection of supplementary materials for this article, available from the publisher (<http://www.tandf.co.uk>), includes the following items. PROCHECK validation reports for structures 1PP9 and 1PPJ. SFCHECK validation reports for structures 1PP9 and 1PPJ. Set of figures laid out for cross-eyed stereo viewing. Scheme and description of the Q-cycle mechanism. Secondary structure diagram for bovine cytochrome *b*. Table of interaction distances between stigmatellin and the protein. Expanded Figure 5 with 7 views, one per page: stereodiagram of space-filling model of cytochrome *b* helix A backbone with intercolated water molecules W3 and W5. Stereo views of omit map density for antimycin in 1PPJ. Stereo views of omit map density for critical residues in 1PPJ C:Ser35, C:Lys227, C:His221-Pro222 (*cis*-peptide), C:His345-Pro346 (*cis*-peptide), D:Gly73-Pro74 (*cis*-peptide). List of standard rotamers referred to, defined by side-chain dihedral angles: VRML views of Figures 1, 5, and 6 with electron density to allow examination from any angle.

<sup>‡</sup> <http://fsrv1.bmc.uu.se>

**Table 1.** Statistics from the structure determination process

	1 PP9	1PPJ
Protein database entry	Stigmatellin	Stigmatellin, antimycin
Inhibitors co-crystallized		
<i>A. Data reduction</i>		
Unit cell dimensions	139.12 × 171.06 × 227.20 Å	128.53 × 168.75 × 231.53 Å
Solvent content	58.2%	54.7%
$V_M$	2.97	2.74
X-ray wavelength <sup>a</sup>	0.99200	0.97977, 1.0000, 1.1000, 1.1808
Unique reflections	312369	285923
Resolution range (Å) <sup>a</sup>	50–2.1 (2.18 – 2.10)	250.–2.100 (2.15–2.10)
Optical resolution <sup>b</sup>	1.72 Å	1.75 Å
Completeness	97.2% (83%)	98.1% (94.3%)
Data redundancy	5.9	5.630
$R_{\text{merge}}$ on $I$ :	0.12 (>1.0)	0.149 (0.879)
$\langle I/\Sigma I \rangle$	10.9 (1.037)	18.6890 (2.819)
<i>B. Refinement</i>		
Resolution	24.99–2.10 (2.15–2.10)	93.53–2.10 (2.15–2.10)
Data cutoff ( $\sigma_F$ )	0.0	0.0
Completeness	97.3 (91.9)	97.7% (90.3%)
# Reflections	305496 (19066)	285060 (16565)
$R$ value	0.250 (0.40)	0.224 (0.33)
Free $R$ value	0.287 (0.40)	0.260 (0.38)
Number of atoms used		
Protein atoms	31493	31181
Heterogen atoms	1005	962
Solvent atoms	1461	1406
$B$ values		
From Wilson plot	27.3 Å <sup>2</sup>	33.50 Å <sup>2</sup>
Mean atomic $B$ value	46.9 Å <sup>2</sup>	50.20 Å <sup>2</sup>
Anisotropic $B_{11}, B_{22}, B_{33}$	15.35, –0.55, –14.81 Å <sup>2</sup>	12.34, –3.71, –8.63 Å <sup>2</sup>
ESD (cross-validated) <sup>c</sup>		
From luzzati plot <sup>c</sup>	0.32 Å (0.39 Å)	0.28 Å (0.35 Å)
From sigma <sup>c</sup>	0.43 Å (0.47 Å)	0.33 Å (0.38 Å)
Rms deviations from ideality		
Bond lengths	0.007 Å	0.006 Å
Bond angles	1.50°	1.4°
Dihedral angles	21.8°	21.8°
Improper angles	1.02°	0.94°
<i>C. Validation</i>		
Residues in “most favored” region of Ramachandran	92.1%	92.4%
Residues in Ramachandran “disallowed” region	0.2%	0.2%
Bad contacts/100 residues	0.5	0.3
Overall $G$ -factor (PROCHECK):	0.4	0.4
Real-space $R$ -value	0.155	0.148
Real-space correlation coefficient	0.909	0.921

<sup>a</sup> Statistics in the highest resolution shell are given in parentheses.

<sup>b</sup> Optical resolution is defined in references.<sup>47,48</sup>

<sup>c</sup> Estimated std. dev. of atomic coordinates. Cross-validated estimates of ESD are given in parentheses.

cytochrome  $c_1$ . The redox-active ectodomains of the ISP and cytochrome  $c_1$  together with subunit 8 (acidic “hinge protein”) make up the membrane extrinsic portion on the external or “P” side of the membrane, while the two largest subunits (“core” proteins<sup>53</sup>) and subunit 6 make up the extrinsic part on the “N” side. Subunit 11 is peripherally bound to the transmembrane domain<sup>46</sup> and readily dissociable after solubilization in DM. It is not present in this crystal form.

Table 2 lists the number of residues modeled for each subunit of each monomer of the two structures discussed here. It also defines the chain letters for the ten subunits in each of two monomers: Chains A to J are subunits 1 to 10 of the “first” monomer, while N to W are the corresponding subunits in the second monomer. The hemes and iron–sulfur clusters are numbered starting at 501 in the same chain to which they are linked. Water molecules are

numbered starting at 1, ligands present at the same place on both monomers are labeled starting at 2001 for monomer 1 and 3001 for monomer 2, and ligands without symmetry mates are numbered starting at 4001.

The 11-subunit bovine  $bc_1$  complex contains 2166 residues per monomer (Table 2),<sup>54</sup> and the 10-subunit preparation used here has 2110 of these. Due to omission of disordered areas, the final structures contain about 2009 residues in each monomer, or 95% of the residues present. The model is lacking the first 17 residues of subunit 2, the first 14 residues of cytochrome b, the first 11 of subunit 6, the first 12 of subunit 8, about half of subunit 9, and smaller sections elsewhere. Monomer 1 of 1PPJ has fewer residues because it is lacking the first 29 residues of subunit 10, which were disordered. Poorly ordered residues that are likely to have mistakes in the current model include

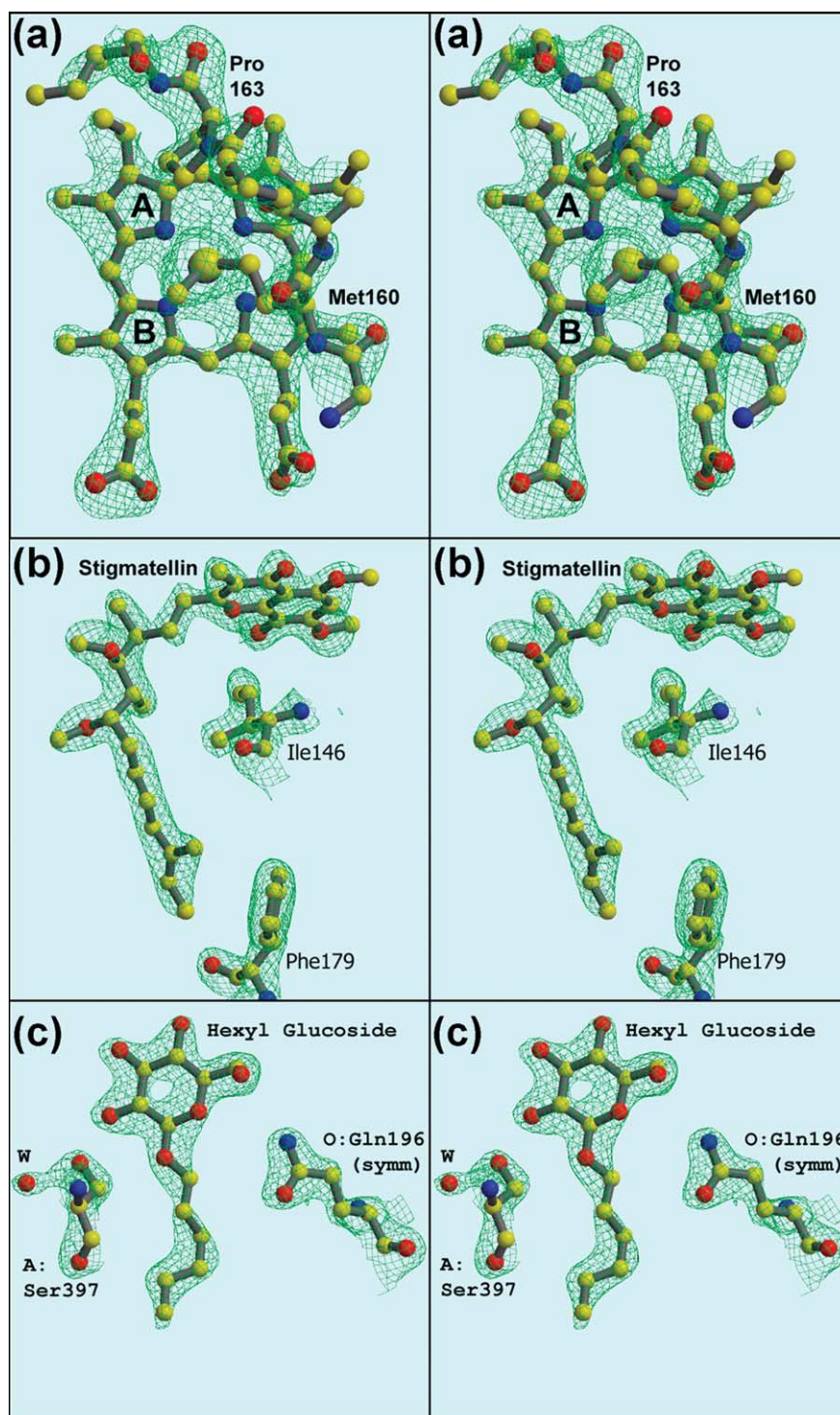


**Figure 2.** Representative density in well-ordered parts of the structure. (a). Heme-ligand met160, showing chirality about the S<sup>δ</sup> atom. (b) Stigmatellin. (c) Hexyl glucoside molecule sandwiched in a crystal contact. The maps are  $2F_o - F_c$  calculated from data between 15 Å and 2.1 Å, sharpened with  $B = 20$ , and contoured at  $2.3\sigma$  (a),  $2.0\sigma$  (b), or  $1.8\sigma$  (c); from structures 1PP9 (a) or 1PPJ (b), (c).

the interdomain linkers of subunits 1 and 2 (A/N 223–230, B/O 230–233); E:79–80 E:178–190; and F109–110.

The entire stigmatellin molecule is well ordered in the current structures, with all but two atoms (the methoxy carbon C5A and final carbon of the tail) covered by  $2F_o - F_c$  density at a contour level of  $2.0\sigma$

(Figure 2(b)). The stereochemistry of the four chiral centers and the planarity at the isoprenoid unit are clear, and are consistent with what is known from chemical investigations.<sup>55</sup>

Modeling of the lipids and detergents in these structures is not yet complete, and will be described in a later paper. At present, there are five

**Table 2.** Model completeness by subunit

Subunit	Number of residues Actual	Modeled in structure			
		1 PP9		1PPJ	
		Monomer #1	Monomer #2	Monomer #1	Monomer #2
1 "core" 1	446	A442	N442	A 441	N 441
2 "core" 2	439	B423	O424	B 424	O 423
3 Cytochrome <i>b</i>	379	C365	P370	C 365	P 365
4 Cytochrome <i>c</i> <sub>1</sub>	241	D241	Q241	D 241	Q 241
5 ISP	196	E196	R196	E 196	R 196
6	110	F 99	S 99	F 99	S 99
7	81	G 73	T 74	G 73	T 74
8 "hinge"	78	H 66	U 66	H 66	U 66
9 signal	78	I 42	V 42	I 43	V 43
10	62	J 62	W 62	J 32	W 61
11	56	K 0	X 0	K 0	X 0
Sum	2166	2009	2016	1980	2009

For each subunit is given the actual number of residues present in the complex based on sequence, and the number of residues modeled in each monomer of the two structures presented here. The chain letters assigned to each subunit in each monomer are also indicated. Major differences are due to the lack of subunit 11 in the crystals and disorder of the first 30 residues of subunit 10 in chain J of 1PPJ.

phospholipids in 1PP9 and four in 1PPJ. One of the best ordered (residues 2007 and 3007; with phosphate H-bonding Tyr103 and Tyr104 of cytochrome *b*) is in the position of one of the lipids in the chicken *bc*<sub>1</sub> structures (e.g. 2BCC) and is also conserved in the yeast *bc*<sub>1</sub> complex (1KB9, 1P84). Phospholipids 2006 and 3006 correspond to the "interhelical lipid" described in the yeast *bc*<sub>1</sub> complex,<sup>52</sup> at the coming-together of transmembrane helices from subunits 3, 4, 5, and 10. As described by Iwata,<sup>56</sup> there are two cardiolipin molecules in the bovine complex where one was modeled in yeast (1KB9).

Six hexyl glucoside (HG) molecules have been modeled in 1PP9, and nine in 1PPJ. For the most part these are poorly ordered and may be misidentified, however in 1PPJ there is one hexyl glucoside that is exquisitely defined by the density (Figure 2(c)). The hexose ring is pinned in a crystal contact between helix  $\alpha M^{\dagger}$  of chain A (at the level of 393–394) and the imidazole ring of O:His192 in a symmetry-related dimer, presumably accounting for the good order. In addition there are H-bonds from O2 of the sugar to A:Ser397 (shown) and from O6 to A:Glu394. This well-ordered detergent is seen in all crystals examined so far that have cell edge  $a=128$  Å, but in the looser lattice of 1PP9 this contact does not occur and the detergent is disordered. In one crystal with cell edge  $a \sim 120$  Å (not shown) this detergent is absent and O:His192 of the sym-related molecule packs directly against helix  $\alpha M$  of chain A. Thus the detergent seems to be the "shim" which accounts for the frequent occurrence of the  $a=128$  Å cell edge after partial dehydration of the crystals.

As expected in the presence of stigmatellin, the ISP is in the proximal or "b" position, with a hydrogen bond between His161 and stigmatellin, which is bound in cytochrome *b*. The significance of

<sup>†</sup> Secondary structure nomenclature for subunits 1 and 2 is defined in Figure 5 of Xia *et al.*<sup>46</sup>

this H-bond has been described in a recent note.<sup>57</sup> The methionine axial heme ligand in cytochrome *c*<sub>1</sub> has "R" chirality at the S<sup>δ</sup> atom, as in the chicken 1BCC or yeast 1EZV structures (Figure 2(a)). The heme planes of heme *b<sub>H</sub>*, heme *b<sub>L</sub>*, and cytochrome *c*<sub>1</sub> are at angles of 25–26°, 5–6°, and 14–16° to the membrane normal, respectively. The orientation of the hemes about their pseudo-2-fold axis is unambiguous and is the same as originally modeled in the chicken structure 1BCC. *cis*-Peptide linkages are present at the peptide bonds involving Pro222, Pro436 (cytochrome *b*) and Pro74 (cytochrome *c*<sub>1</sub>) as the (*i* + 1)th residue. The assignment is unambiguous for these three residues, and has been verified in cross-validated  $\sigma A$ -weighted  $F_o - F_c$  omit maps calculated for 1PPJ omitting residues in a sphere of radius 3 Å around the residue and calculated between 93.5 Å and 2.2 Å resolution. Pro21 in subunit 2 is also modeled as a *cis* peptide, but the position of His20 is not well defined by the density so this is likely to be in error. No other *cis*-peptide linkages were found.

### Heme-binding helix bundle and heme *b<sub>H</sub>*

As deduced from sequence analysis<sup>58–60</sup> and described in previous structures,<sup>20,46,52</sup> cytochrome *b* is primarily  $\alpha$ -helical, with eight transmembrane helices labeled **A–H** and four "surface" helices labeled  $\alpha a$  (before helix **A**),  $\alpha cd_1$  and  $\alpha cd_2$  (between helices **C** and **D**), and  $\alpha ef$  (between helices **E** and **F**). There is one small  $\beta$ -sheet consisting of two antiparallel strands from the linker regions before helices **A** and **E**, which will be described below in connection with the antimycin site.

The two hemes are located within a four-helix bundle consisting of helices **A**, **B**, **C**, and **D**; with the high potential heme (heme *b<sub>H</sub>*) toward the N side and low potential heme (heme *b<sub>L</sub>*) toward the P side of the membrane. Both hemes have bis-histidyl ligation, with the histidine ligands provided by helices **B** and **D** (His83, 97, 182, and 196 in the

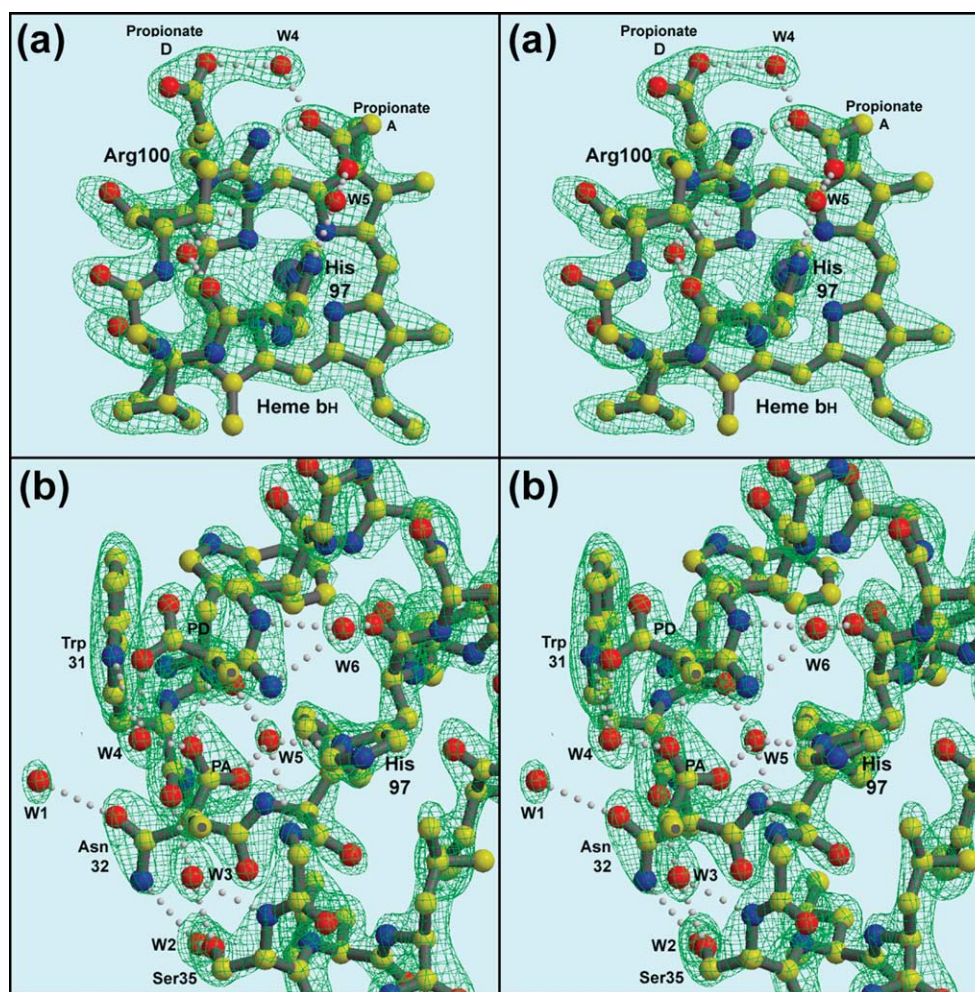


**Figure 3.** H-bonding around the high potential cytochrome *b* heme. (a) Heme *b<sub>H</sub>* viewed from helix *B*. Water *W4* bridges between the two heme propionate side-chains, while *W5* bridges between a propionate and the heme axial ligand His97. Arg100 interacts directly with this “bent” propionate, and *via* unlabeled water molecule *W6* with the carbonyl O of His97. *W5* is also H-bonding with backbone atoms of helix *A*, which has been removed from this view for clarity. (b) The same region viewed from the heme position, looking toward helices *A* and *B*. The heme is removed except the two propionate side-chains. Intercalation of water molecules *W3* and *W5* in the helical backbone of helix *A* can be seen. Water molecules *W1*–*3* are discussed in the text in connection with antimycin binding. The map is a  $2F_o - F_c$  map calculated from data between 15 Å and 2.1 Å, sharpened with  $B = 20$ , and contoured at  $1.8\sigma$  (a) or  $1.7\sigma$  (b).

bovine sequence). In addition there are four conserved glycine residues in helices *A* and *C* where the heme ring makes a close contact (Gly34, 48, 116, and 130).

Heme *b<sub>H</sub>*, with axial ligands His97 and His196, is distinctly curved: pyrrole rings† *A* and *C* bend toward the His97 side while rings *B* and *D* are nearly in a straight line with the iron (forming the axis of curvature). Pyrrole rings *B* and *D* lie along the axis of the four-helix bundle with rings *A* and *C* on the sides, inserting between the helices that comprise the bundle. Ring *A*, exposed between helices *A* and *D*, contributes to the antimycin binding site (below).

† The pyrrole rings of heme referred to here as *A*, *B*, *C*, and *D* correspond to protoporphyrin rings conventionally labeled IV, I, II, and III.

As reported,<sup>20,52</sup> the propionate on the *A* ring is bent sharply back toward the axial ligand His97, making an ion-pair with the guanidino group of Arg100 (bovine sequence numbering). We can see now (Figure 3) that this ion pair involves only one of the carboxylate oxygen atoms and NH1 of the guanidino group of R100 (distance 2.8 Å), but that the propionate in addition binds two very well-ordered water molecules (Figure 3 and Table 3). The same propionate oxygen that ion-pairs with R100 has a second bond (2.8 Å) to an entity modeled as water *W4*, whose other ligands are the other (*D*) propionate and Ser205 O<sup>γ</sup>. The other oxygen of the *A* propionate is separated by 3.3 Å from the NH2 atom of Arg100, but makes a very strong (2.44 Å) bond with another stable water molecule *W5* which bridges between this propionate and the N<sup>δ</sup> atom of the heme axial ligand His97. This water

**Table 3.** Potential H-bonding partners for six highly-ordered water molecules in the region of heme  $b_H$  and the  $Q_i$  site

Label	Water res. (C, P)		H-bond Res.	Partner		Distance		B-value	
				Num	Atom	C	P	C	P
W1	119	959	** Antimycin		O2	2.6	2.6	44	38
			** LYS	227	NZ	2.6	2.6		
			** SER	28	O	3.1	2.9		
			** ASN	32	OD1	3.2	3.3		
W2	1008	214	** SER	35	OG	2.7	3.0	29	32
			** ASN	32	ND2	2.8	2.8		
			** ASP	228	O	3.0	2.7		
W3	222	28	** Antimycin		N1	3.2	3.2	25	32
			** Antimycin		O1	2.9	2.8		
			** TRP	31	O	2.7	2.7		
			** ASN	32	O	3.2	3.2		
			** SER	35	N	2.8	2.8		
			** SER	35	OG	3.0	2.9		
W4	168	109	** SER	205	OG	2.5	2.5	27	31
			** HEM	502	O2A	2.8	2.8		
			** HEM	502	O1D	2.7	2.7		
W5	2	1	** HEM	502	O1A	2.5	2.6	33	30
			** TRP	30	O	2.8	2.7		
			** HIS	97	ND1	2.9	2.8		
			** PHE	33	N	3.1	3.3		
			** GLY	34	N	3.1	3.4		
			** ARG	100	NH1	3.5	3.4		
			** ARG	100	NH2	3.5	3.2		
W6	108	35	** HIS	97	O	2.6	2.7	31	32
			** ARG	100	NE	3.2	3.1		
			** ARG	100	NH2	3.2	3.0		
			** GLY	101	N	3.3	3.4		

\*\*—Potential hydrogen bond.

also makes bonds with the carbonyl oxygen of Trp30 and backbone N of C33 in the A helix. This rigid framework presumably serves to fix the plane of the heme-ligand histidine, and may be partly responsible for the heme curvature mentioned above. The sharply bent A propionate arm also forms one surface of the  $Q_i$  binding site (see below), and may be on the path for electron transfer between heme  $b_H$  and quinone at that site. The other propionate, on the D pyrrole ring of heme  $b_H$ , H-bonds with one carboxylate oxygen to the side-chains of Ser106 and Trp31, and with the other to the backbone nitrogen of Asn206 and to the water molecule W4 mentioned above. This arrangement of the propionates, Arg100, the two water molecules, and their ligands is the same in the presence or absence of antimycin, and is seen also in the yeast  $bc_1$  structures (e.g. 1P84), so it is likely to be a static arrangement. However, if at some point in the reaction cycle the A propionate could be released to straighten out, it would put the carboxylate in the  $Q_i$  site, as a possible ligand for a quinone species there, as well as modulating the charge density near the heme iron and curvature of the macrocycle.

Ser205, one of the ligands for strongly ordered water W4, is replaced by Asn221 in *Rb. sphaeroides*. It has been proposed that the  $O^{\delta 1}$  atom of Asn221 occupies the position of W4 bridging between the two heme propionates, positioning the  $N^{\delta 2}$  atom to serve as a ligand for quinone in the bacterial complex.<sup>33</sup>

### Molecular configuration of bound antimycin

The antimycin in structure 1PPJ is very well ordered, with average  $B$ -factors in the two monomers of  $41.5 \text{ \AA}^2$  and  $43.6 \text{ \AA}^2$ , barely above that for the backbone of cytochrome b ( $39.0, 40.9$ ) and lower than the average  $B$ -factor for the structure ( $50.2 \text{ \AA}^2$ ). The electron density is correspondingly good, and there is little ambiguity in the placement of any of the atoms except the tips of the alkyl and acyl side-chains. The degree of order is greatest on the formylamino-salicylamide portion, which is well defined in  $2F_o - F_c$  maps contoured at  $2.1\sigma$  (Figure 1(b)), and decreases through the dilactone ring and into the alkyl and acyl side-chains at the other end. At  $1.5\sigma$  (not shown) the acyl chain is visible through C3 and shows the methyl branch to be at the 2 position as reported<sup>42</sup> rather than the 3 position as previously believed, and at  $0.9\sigma$  (Figure 1(c)) there is weak density for C4 in one monomer, tentatively modeled in Figure 4(b) and (c) for completeness. The alkyl side-chain has density through the fifth carbon when contoured at  $0.9\sigma$  (Figure 1(c)).

The dihedral angles of the formylamino group<sup>38</sup> are approximately  $0^\circ$  ( $\Theta_1$ ) and  $180^\circ$  ( $\Theta_2$ ), in agreement with values found in an energy-minimized structure.<sup>38</sup> Similar values were found in the small-molecule structure<sup>42</sup> and for the bound inhibitor in structure 1NTK. These angles put the formylamino group in the plane of the salicyl ring, directed away from the OH and carboxylate groups

and toward Lys227 of cytochrome b (Figure 6). The observation<sup>40</sup> that a methyl group at position 4 but not at position 5 diminishes binding of antimycin analogs is consistent because the methyl at position 4 (compound 17) would prevent the formylamino group from taking on this conformation.<sup>38</sup>

The dihedral angle  $\Theta_3$  between the phenyl ring and carbonyl carbon of the salicylate moiety is approximately 180°; that is the amide group is rotated 180° relative to the salicyl ring from the small-molecule structure. This means that the internal H-bond between the phenolic OH and amide carbonyl oxygen, which was proposed to be important for inhibition,<sup>38</sup> and which was observed in the small-molecule structure<sup>42</sup> (indicated in Figure 1(a)), is actually not present in the enzyme-bound form (Figure 1(b) and (c)). The observed orientation of the amide moiety with respect to the salicylate ring is contrary to that modeled in structure 1NTK. This and other discrepancies will be considered in Discussion.

The 9-membered dilactone ring of antimycin is puckered with alternating members directed up and down except C<sup>β</sup> of the threonine†, which is between members facing up and down. The chirality of the chiral centers meshes with the puckering in such a way that the three bulky substituents as well as one methyl side-chain (C5 of the valeric acid moiety) project equatorially, i.e. more or less in the plane of the dilactone ring, while the two carbonyl oxygen atoms project perpendicular to the ring. The other methyl group (C<sup>γ</sup> of threonine) projects at an intermediate angle. The planes of the ester and amide substituents and the salicyl ring are nearly perpendicular to the dilactone ring. This differs from the small-molecule structure, in which the plane of the salicyl ring and amide are approximately 45° from that of the dilactone ring (compare Figure 1(a) and (b); in both of which the salicylamide is in the plane of the picture).

### The antimycin-binding site

Figure 4 shows the make-up of the antimycin

† There are different conventions for naming the atoms in antimycin, so we have tried to specify atoms from a chemical standpoint rather than by name. The protein database maintains two versions of antimycin, AMY (from 3BCC) and ANY (introduced with 1PPJ). These have the same atom names, but in ANY two additional carbon atoms have been added to the end of the acyl chain to allow for the possibility that it is heptyl, and the methyl group on the acyl chain has been moved from the 3 to 2-position in accordance with recent results.<sup>42</sup> In the Cambridge Structure Database of small molecule structures there is (CCDC # 125007) from the work of Deisenhofer's group,<sup>42</sup> which uses different atom names. The PDB entry 1NTK uses the atom names from the Cambridge Database but the residue name (AMY) from the Protein Data Bank. The atom names here, where used in the text and in Figure 1 and Table 4, are from ANY of 1PPJ.

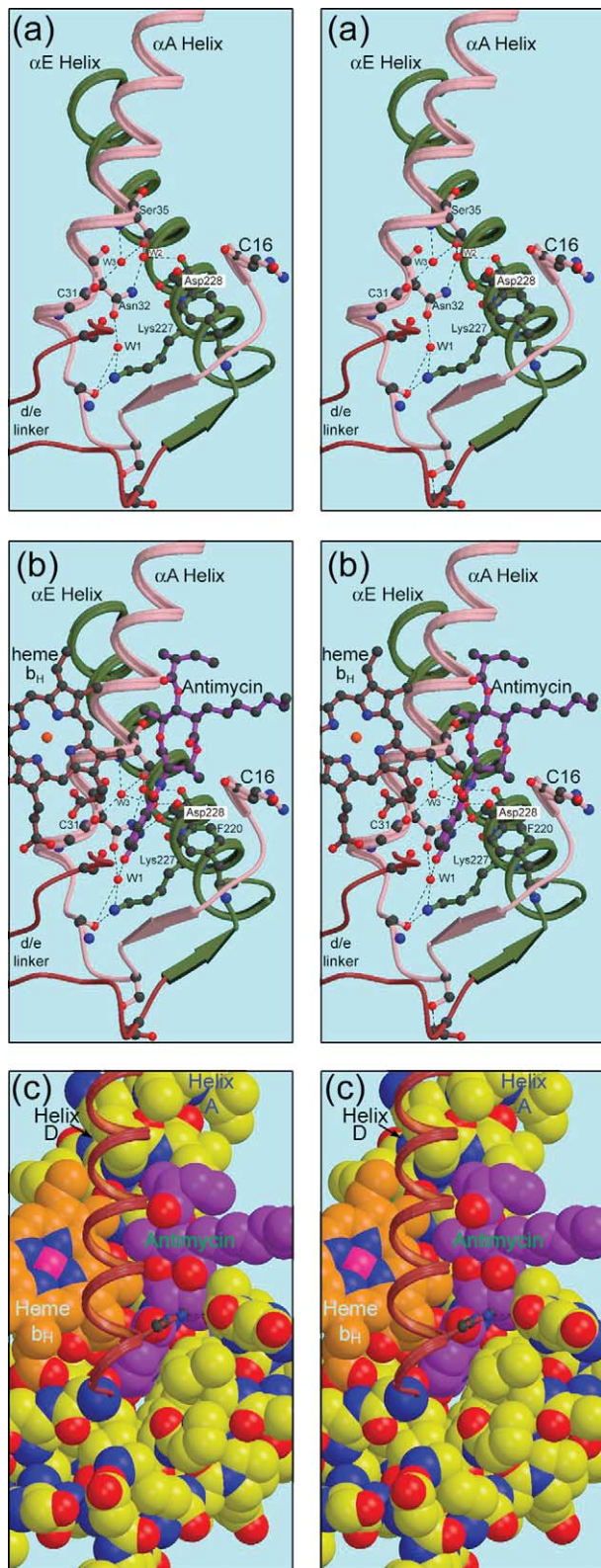
binding site in different levels of dissection, and Table 4 lists contacts between antimycin and the protein. Briefly, the antimycin headgroup is found in a pocket which is bounded by helices  $\alpha A$ ,  $\alpha D$ ,  $\alpha E$ , and  $\alpha a$ ; as well as the edge of heme  $b_H$  exposed between helices  $\alpha A$  and  $\alpha D$  of the four-helix bundle. Strong hydrogen bonds are formed directly with Asp228 in helix E and *via* ordered water molecules to Lys227 in helix E and Ser35 in helix A.

Figure 4(a) shows the underpinnings of the antimycin binding site in helices A and E. These helices cross at an angle, with Van der Waals contacts at the crossing between the side-chains of Leu43 and Leu239 (not shown). The N-terminal (N-side) ends of these helices are connected by  $\beta$ -bridges between residues in the sequence preceding the helices: residues 21, 23, and 25 in the region before helix A make backbone H-bonds with residues 221, 220, and 218 before helix E. In addition, a strong hydrogen bond between the side-chains of Asp216 and Ser25 hold these two residues together. These  $\beta$ -bridges are represented by the antiparallel arrows in Figure 4, and together with helices A and E they bound a triangular volume that encloses the Q<sub>i</sub> site. Another connection between the A and E helices is made by Lys227 in the E helix which H-bonds with the backbone oxygen of residue 27 and a highly ordered water molecule attached to helix A. These bonds are part of a more extensive H-bonding chain that is involved in antimycin binding but is present in both structures 1PPJ (with antimycin) and 1PP9 (without). This chain is shown in stereo in Figure 4(a). Lys227 and the first water (W1) are bonded to each other and to the carbonyl oxygen of residue 27. W1 is also bonded to O<sup>γ1</sup> of Asn32. N<sup>γ2</sup> of this residue H-bonds a second water (W2) which in turn bonds to Ser35O<sup>γ</sup> and to the carbonyl oxygen of Asp228, further linking the A and E helices. A third water (W3) also bonds with Ser35O<sup>γ</sup> and additionally with the backbone O and N of residues 31 and 35, respectively (Figure 4(a)). As these latter two atoms would normally be involved in the  $\alpha$ -helical H-bonding of helix A, W3 can be seen as "intercalated" into the helix‡.

In addition to the A and E helices, both the D helix and the  $\alpha a$  surface helix contribute to the Q<sub>i</sub> site. Helix D is omitted in Figure 4(a) and (b) for

‡ In fact the helical bonding is interrupted, with normal  $\alpha$ -helical bonding involving the N atom of residues after 35, 3/10 helical bonding involving the O of residues before 31, and no strong helical bonds of either sort involving O of residue 31 or 32 and N of residue 35. The distance from 31O to 35N is 5.1 Å, and to 34N 4.1 Å. The intercalated water W3 is well ordered, with B-factors 25 Å<sup>2</sup> and 32 Å<sup>2</sup> in 1PPJ (but 30 Å<sup>2</sup> and 46 Å<sup>2</sup> in 1PP9), well below average for the structure, and with density in 2F<sub>o</sub> - F<sub>c</sub> maps 3.9 to 4.7σ. The heme-propionate-to-axial-ligand-bridging water W5 mentioned in connection with heme  $b_H$  can also be seen as intercalated, with a short H-bond to 33 O, but it is equally close to 33 N and 34 N, with neither being as close as 35 N is to W3 (Table 3).

1261  
1262  
1263  
1264  
1265  
1266  
1267  
1268  
1269  
1270  
1271  
1272  
1273  
1274  
1275  
1276  
1277  
1278  
1279  
1280  
1281  
1282  
1283  
1284  
1285  
1286  
1287  
1288  
1289  
1290  
1291  
1292  
1293  
1294  
1295  
1296  
1297  
1298  
1299  
1300  
1301  
1302  
1303  
1304  
1305  
1306  
1307  
1308  
1309  
1310  
1311  
1312  
1313  
1314  
1315  
1316  
1317  
1318  
1319  
1320  
1321  
1322  
1323



**Figure 4.** Structure of the Q<sub>i</sub> site and interaction with bound antimycin. The Q<sub>i</sub> site lies in a triangular volume formed by helices B and E crossing at an angle (a) The N-side (N-terminal) ends of these helices are held together by  $\beta$ -type H-bonding between residues just preceding the helices (arrows in cartoon) which bounds the third side of the volume, and by Lys228 of helix E which H-bonds with a backbone O of residue 27, and to a

clarity (the view is from the position of helix D), but the linker polypeptide connecting helix D to helix E is shown. Ser205, early in the D/E linker is shown as ball-and-stick. This residue has been implicated in quinone binding at this site,<sup>24,33,52,61</sup> and will be discussed further below. The  $\alpha$ -a surface helix, starting with residue 15 is shown. This turn borders on the Q<sub>i</sub> site, and there is some indication that the carbonyl oxygen atoms of residue 16 or 17 may H-bond with the side-chain of His201. Unfortunately this region is poorly ordered in both monomers of these crystals, and its contribution to the Q<sub>i</sub> site can better be seen in the yeast (e.g. 1KB9) or chicken (3BCC) structures.

In Figure 4(b) antimycin and heme *b<sub>H</sub>* are added to the picture, and Figure 4(c) shows a space-filling model of everything represented in Figure 4(b) and also adds helix D as a thin ribbon. The H-bonding contacts of antimycin can be seen in Figure 4(b) and, in greater detail, in Figures 5 and 6. The only direct H-bonds with the protein involve conserved Asp228, the carboxylate of which binds to the phenolic OH and the formylamino NH. It seems reasonable to assume that Asp228 is deprotonated at the pH of the crystal, and serves as H-bond acceptor in both these bonds. The phenolic OH also has an H-bond with the intercalated water W3, as well as the intramolecular H-bond mentioned above with the amide NH. Following the reasoning

water molecule bonded to that atom and to Asn32 O $\gamma$ <sup>1</sup> of helix A. These bonds are part of a more extensive H-bonding chain involving also Trp31, Ser35 and two other water molecules. In (b) antimycin (magenta bonds) and heme *b<sub>H</sub>* (orange bonds) are added. The methyl and propionate substituents of the "A" ring of heme protrude from the four-helix bundle between helices A and D (helix D removed for clarity), forming part of the surface of the binding site. The formylaminosalicylate headgroup of antimycin inserts into the triangular volume described above, sandwiched between Phe220 of helix E and the heme propionate, and H-bonding with Asp228 and (*via* another water) Lys227. In (c) the protein elements shown in (a) are rendered as space-filling model to show the surface of the binding site. Antimycin (magenta carbon atoms) and heme *b<sub>H</sub>* (orange carbon atoms) are also space-filled to show the intimate contact between these moieties and the snug fit of the antimycin headgroup in the protein. The binding pocket is completed by the  $\alpha$ -a surface helix (shown here starting with residue 15) and the D transmembrane helix, left as a ribbon for clarity. There may be H-bonds involving His201 in helix D with the amide carbonyl oxygen of antimycin and with a backbone oxygen in the  $\alpha$ -a helix. At the lower extreme of antimycin is the aromatic ring, viewed edge-on and inserted between the bent propionate of heme *b<sub>H</sub>* and Phe220 in helix E. The carbonyl oxygen of the amide linkage is directed toward the viewer, seen beneath His201 of helix D. Higher up, the alkyl side-chain extends to the right into the lipid-filled cleft. At the top is the acyl group, with the ester carbonyl oxygen directed towards the viewer. Note the close contact with heme *b<sub>H</sub>*, involving not only the aromatic ring of antimycin but also part of the dilactone ring.

1324  
1325  
1326  
1327  
1328  
1329  
1330  
1331  
1332  
1333  
1334  
1335  
1336  
1337  
1338  
1339  
1340  
1341  
1342  
1343  
1344  
1345  
1346  
1347  
1348  
1349  
1350  
1351  
1352  
1353  
1354  
1355  
1356  
1357  
1358  
1359  
1360  
1361  
1362  
1363  
1364  
1365  
1366  
1367  
1368  
1369  
1370  
1371  
1372  
1373  
1374  
1375  
1376  
1377  
1378  
1379  
1380  
1381  
1382  
1383  
1384  
1385  
1386

1387  
1388  
1389  
1390  
1391  
1392  
1393  
1394  
1395  
1396  
1397  
1398  
1399  
1400  
1401  
1402  
1403  
1404  
1405  
1406  
1407  
1408  
1409  
1410  
1411  
1412  
1413  
1414  
1415  
1416  
1417  
1418  
1419  
1420  
1421  
1422  
1423  
1424  
1425  
1426  
1427  
1428  
1429  
1430  
1431  
1432  
1433  
1434  
1435  
1436  
1437  
1438  
1439  
1440  
1441  
1442  
1443  
1444  
1445  
1446  
1447  
1448  
1449

**Table 4.** Residues surrounding antimycin at the Q<sub>i</sub> site

	Helix A and water molecules (W)				Helices D and E				Heme b <sub>H</sub>			
	Protein atom	Anti atom	Distance (Å)		Protein atom	Anti atom	Distance (Å)		Heme atom	Anti atom	Distance (Å)	
			C	P			C	P			C	P
ALA17	O	C10	3.6	3.7				HEM502	N2	3.8	3.8	
ILEZ7	CD1	O2	3.5	3.5	MET190	CG	C23	HEM502	C9	3.8	3.7	
TRP31	O	N1	3.4	3.4	MET194	CG	O9	HEM502	O4	3.2	3.2	
ASN32	O	C27	3.9	3.9	LEU197	CD1	O4	HEM502	C20	3.3	3.3	
GLY34	O	C27	3.9	4.0	SER205	OG	C4	HEM502	O7	3.7	3.7	
SER35	CA	O7	3.0	3.1				HEM502	C27	3.9	3.9	
GLY39	CA	C27	3.8	3.7	PHE220	CE1	C1	HEM502	C5	3.8	3.9	
SER35	CA	O7	3.0	3.1				HEM502	C27	3.9	3.9	
GLY38	CA	C27	3.8	3.7	PHE220	CE1	C1	HEM502	C5	3.8	3.9	
LEU41	CD2	C25	3.9	3.7	TYR224	CD1	O2	HEM502	C6	3.8	3.9	
W3	O**	O1	2.9	2.8	ASP228	OD1**	N1	HEM502	C7	3.9	4.0	
W1	O**	O2	2.6	2.6	ASP228	OD2**	O1	HEM502	C1	3.8	3.8	
"W"	O	O3	2.6	2.8				HEM502	C5	3.7	3.8	
W1203	O	C5	—	3.7				HEM502	C6	3.6	3.6	

For each contact closer than 4 Å is given the residue type, number, and atom; the atom of antimycin, and the contact distance in each monomer. For distances greater than 3 Å, only the closest contact of each protein residue is given. Except for water molecules, all the residues contacting antimycin belong to cytochrome b (chains C and P). The "water" modeled between His201 and antimycin O3 does not account for the density as currently modeled (Figure 6).

above it must be the acceptor in both of these bonds, as its one proton is being donated to Asp228. The formylamino oxygen H-bonds to water W1 discussed above. Otherwise, the contacts appear all to be hydrophobic. Strikingly, no H-bond is made with the dilactone ring or its acyl side-chain.

The substituents of the "A" pyrrole ring of heme b<sub>H</sub> (the bent propionate described above and a methyl group) protrude from the 4-helix bundle between the A and D helices, forming part of the surface of the Q<sub>i</sub> site. The space-filling model in Figure 4(c) illustrates the intimate contact between heme (orange) and antimycin (magenta), consistent with the electronic interactions required to explain the quenching of antimycin fluorescence and the spectral shift of cytochrome b<sub>H</sub> on binding. The aromatic headgroup of antimycin is inserted into a cavity between the bent propionate and Phe220. The aromatic ring of Phe220 is not quite perpendicular to the salicyl ring, the actual angle being 77°. The axial methyl group of the dilactone ring interdigitates loosely with the methyl groups on pyrrole rings A and B of the heme.

**Van der Waals contact with Ser205, a possible ubiquinone ligand**

On the other side of the formylamino-salicyl ring from Asp228, potential H-bonding partners are Ser205 and His201 (Figure 4(b) and (c), Figure 6), both believed to be important in ubiquinone binding at the Q<sub>i</sub> site.<sup>33,52,61,62</sup> Ser205 makes Van der Waals contact with C5 of the salicylate ring, but there is no H-bonding partner on this area of antimycin.

In antimycin analogs lacking the 3-formylamino group, inhibition can be restored by 3 or 5-NO<sub>2</sub> groups, and to some extent by a 5-formylamino group.<sup>41</sup> This has been attributed to a requirement for an electron-withdrawing substituent to increase the acidity of the phenolic OH,<sup>16</sup> however, based on a more extensive set of analogs, Tokutake *et al.* decided that electron-withdrawal did not correlate well with activity, and concluded specific interactions of both the formylamino and phenolic OH with the protein were involved. It seems likely that a nitro group in the 5- position would H-bond Ser205, while one in the 3- position would H-bond Asp228. Super-position of 3 or 5-nitrosalicylate on the salicylate moiety of antimycin in 1PPJ (not shown) results in too-close contacts (1.7 Å and 1.3 Å) of the 3-nitro group oxygen with Asp228 and the 5-nitro group with Ser205. Small adjustments in the positions of these side-chains, or slight repositioning of the ring, could allow a good fit.

Thus H-bonding may be as important as electron-withdrawal in explaining the effects of nitro-substituents. However, in light of our assumption that the phenolic OH is the H-bond donor in the bond with Asp228, it has to be questioned whether the more acidic nitro- compounds, which might be deprotonated at neutral pH, could bind in the same way as antimycin. In fact the detailed inhibition

1450  
1451  
1452  
1453  
1454  
1455  
1456  
1457  
1458  
1459  
1460  
1461  
1462  
1463  
1464  
1465  
1466  
1467  
1468  
1469  
1470  
1471  
1472  
1473  
1474  
1475  
1476  
1477  
1478  
1479  
1480  
1481  
1482  
1483  
1484  
1485  
1486  
1487  
1488  
1489  
1490  
1491  
1492  
1493  
1494  
1495  
1496  
1497  
1498  
1499  
1500  
1501  
1502  
1503  
1504  
1505  
1506  
1507  
1508  
1509  
1510  
1511  
1512

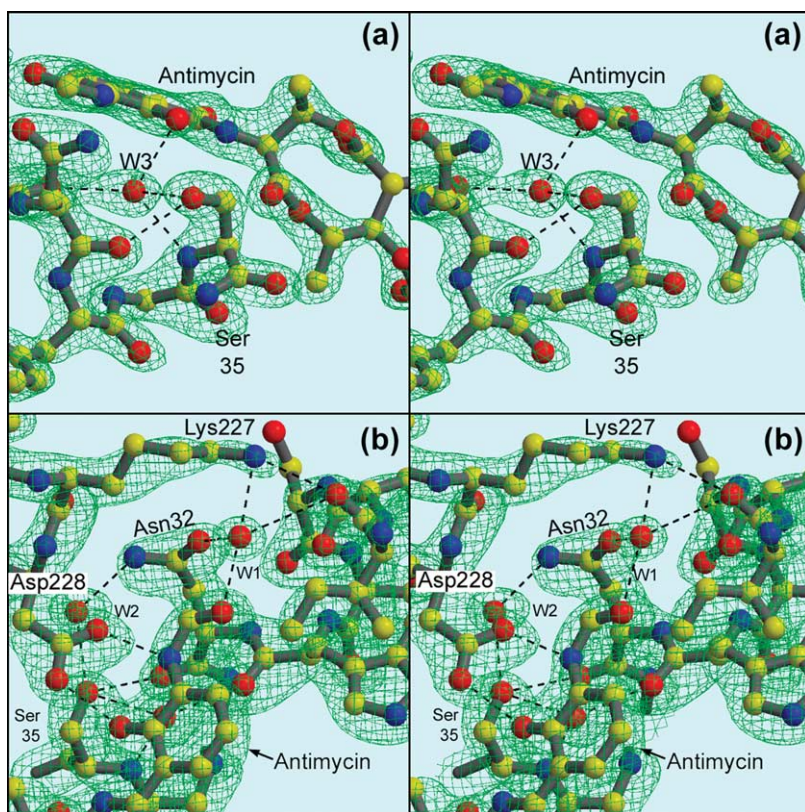


**Figure 5.** Ser35 carbonyl O faces away from antimycin, and Lys227 interacts with antimycin through a water molecule. (a) Ser35 and vicinity: a  $2F_o - F_c$  map contoured at  $1.5\sigma$ . Asp228 has been removed for clarity, and W2 is not shown. (b) Lys227, Asp228, and vicinity: Antimycin is in the front and lower part of the figure, with its formyl-amino oxygen at the center. Water W1 bridges between the formyl-amino oxygen and Lys227N $\epsilon$  at the top of the figure. W1 also makes H-bonds with O $\gamma$ 1 of Ser32 (left) and the carbonyl oxygen of C27 (right). Also visible in this figure, two-point H-bonding of Asp228 to antimycin. In the background is Asn32 with H-bonds stabilizing W1 and W2, and a bond from the latter atom to Ser35. The intercalated water W3 is behind antimycin, barely visible through the salicyl ring, with H-bond to Ser35 indicated. The map is the same as in (a).

pattern of nitrosalicylate compounds has been found to be quite different from antimycin and other 3-formylamino compounds, the nitrosalicylates being ineffective in eliciting either the “double-kill” behavior or oxidant-induced reduction seen with antimycin.<sup>40,63</sup>

### His201 conformation

The most enigmatic part of the structure around the antimycin binding site is the critical conserved residue His201, which is believed to be a ligand for quinone<sup>52,61,62</sup> either directly<sup>61</sup> or indirectly through a water molecule.<sup>52</sup> When contoured at a  $1.5\sigma$  density level (Figure 6(a)) the imidazole ring seems well localized, but poorly shaped for this resolution. His201 here is modeled in a position close to rotamer 5 $\dagger$ , as in all vertebrate cytochrome *bc*<sub>1</sub> structures currently available, and there is really no possibility of modeling it in with a significantly different value of  $\chi$ -1.

The distance from His201N $\epsilon$ 2 to the antimycin O

is 4.20 Å, precluding any significant direct H-bonding. An extra bit of density has been modeled as water, with distances 2.81 Å from the water to the amide carbonyl O of antimycin and 2.63 Å to the Ne2 of His201. In fact, the density is too close to the histidine to be a water molecule. Non-bonded interaction terms in the refinement process have pushed the modeled water outside of the density peak, and displaced His201 slightly from its best fit. When the water is moved to its density peak, the distances are 1.82 to the His201 and 3.07 to antimycin. When the water is removed and the model is subjected to further positional refinement, His201 moves only slightly closer to antimycin, distance 4.12 Å (not shown).

When contoured at a lower level ( $1.0\sigma$ , Figure 6(b)), the density around the imidazole spreads out in a triangular shape and merges with the peak assigned to water. This may result from a mixture of two alternative conformations: one in which the water is present at its density peak but His201 rotates back to be farther from it, and another in which the water is absent and His201 rotates forward toward the water position and bonds directly with antimycin.

The two conformations postulated here, and the presence or absence of a water molecule between the histidine and the Q<sub>i</sub>-site occupant, should not be confused with another interesting difference between available structures. In all the yeast structures presented to date, His202 (corresponding to His201 in the bovine sequence) is positioned close to rotamer 3<sup>c</sup>. A water molecule bridges

$\dagger$  Rotamer numbers used here refer to the lists of rotamers provided with the molecular visualization/modeling program O,<sup>73</sup> with the most frequently-occurring being in each case rotamer 1. Lysine rotamer 26 is an exception, coming from the more extensive collection of rotamers in Lovell *et al.*<sup>67</sup> The actual side-chain dihedrals of the rotamers referred to are as follows: Ser rotamer 1:  $\chi_1 = 63^\circ$ ; Ser2:  $\chi_1 = -62^\circ$ ; His3:  $\chi_1 = -169^\circ$ ,  $\chi_2 = 80^\circ$ ; His5:  $\chi_1 = -59^\circ$ ,  $\chi_2 = 169^\circ$ ; Lys26:  $\chi_1 = -66^\circ$ ,  $\chi_2 = 180^\circ$ ,  $\chi_3 = 67^\circ$ ,  $\chi_4 = 180^\circ$ .

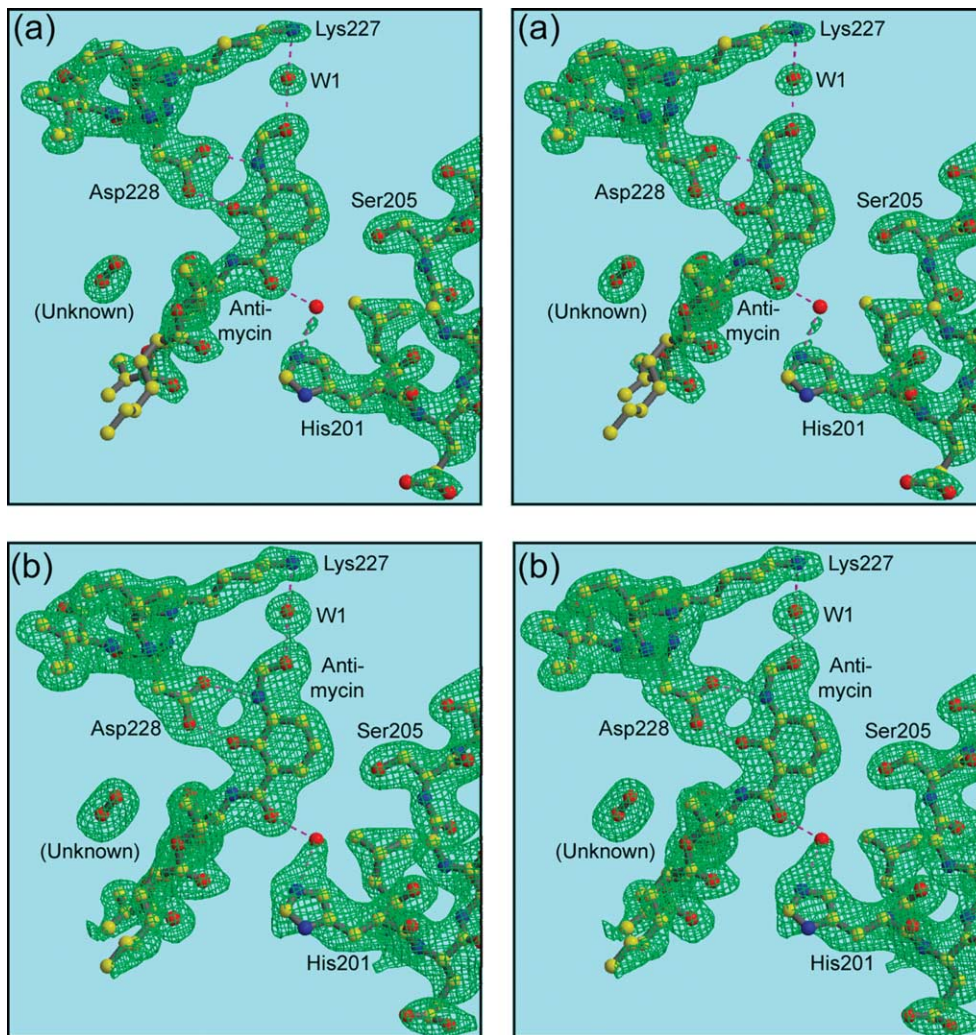


**Figure 6.** His201 and Ser205. The view is nearly the same as Figure 5(b), showing antimycin, Lys227, Asp228 and water 1. Residues behind those have been removed for clarity, and the C terminus of helix D containing His201 and Ser205 is shown. Two different density levels are used to elucidate the interaction of His201 with antimycin and the possible involvement of a water molecule. The maps are  $2F_o - F_c$ , contoured at  $1.5\sigma$  in (a) and  $1.0\sigma$  in (b). Also shown is an unknown molecule modeled as dioxygen (see the text).

between the  $N^{\epsilon 2}$  nitrogen and the carbonyl oxygen of ubiquinone. In the chicken *bc*<sub>1</sub> structures with ubiquinone, His202 is close to rotamer 5, which allows a direct H-bond to ubiquinone. It seems quite reasonable that both these conformations are correct, depending perhaps on pH or ionic strength, and that the direct involvement of a water may be part of the mechanism for uptake of the protons involved in quinone reduction at the  $Q_i$  site. However, that may be, all of the vertebrate *bc*<sub>1</sub> structures available today have His202 (201) in rotamer 5, and all the yeast structures have rotamer 3. At first glance, the bovine structure 1NTZ (with quinone supplemented) seems to be an exception, as the H-bond between quinone and His201 is mediated by a water molecule as in the yeast structures. However, superposition of the chicken and yeast structures shows that in 1NTZ, His201 is in the chicken position (rotamer 5) and the quinone

is deeper in the pocket than in the yeast or chicken structures, making room for the mediating water.

**Unknown molecule in hydrophobic site between dilactone and helix A**

There is a strong density between the dilactone ring of antimycin and helix A which during most of the refinement of the structure was modeled as a water. Since there are no nearby H-bonding partners to account for stabilizing a water molecule in this position, it was removed before submitting the structure to the PDB. However, this leaves a strong peak in difference Fourier maps, indicating that something is there, even if it is not a water molecule. The peak is oblong and about the right size for a diatomic molecule. In consideration of the hydrophobic nature of the environment and the lack of H-bonding partners we think it may be a

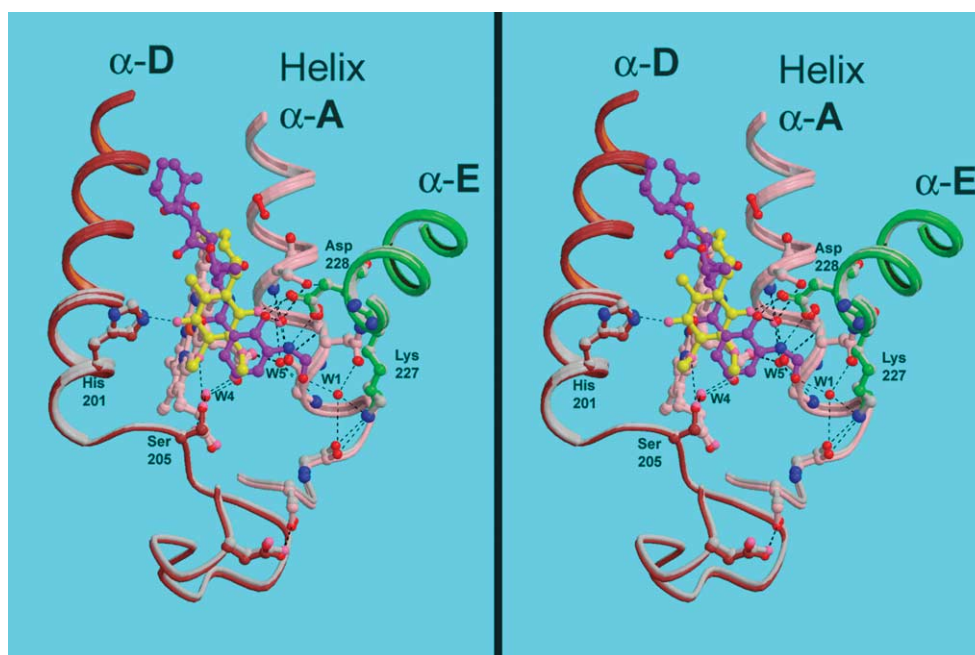


**Figure 7.** Comparison of  $Q_i$ -site residues and ligands in structures 1PPJ and Y21. The two structures were superimposed based on cytochrome b residues 32–51, 79–99, 113–145, 161–201, and 263–300. The backbone is shown for parts of transmembrane helices A (pink), D (red), and E (green), in color for 1PPJ and gray for Y21; as well as some of the linker region preceding helices A and D. Relevant side-chains are drawn with bonds and carbon atoms the same color as the backbone. Water molecules are shown as red spheres for 1PPJ and pink spheres for Y21. Antimycin from 1PPJ is shown as a purple ball-and-stick figure with red oxygen atoms, while ubiquinone from structure Y21 is yellow. Note the relatively invariant positions of the backbone and side-chains, and the positioning of the ubiquinone ring over the amide moiety of antimycin.

non-polar gas such as nitrogen or oxygen. It is modeled as  $O_2$  in Figure 6, and labeled “unknown”. The closest contacts in antimycin are O7 and C11 (3.7 Å and 4.0 Å). The closest contacts in helix A are the carbonyl O of ser35 (4.0 Å) and side-chains of Ile39 and Ile42 (4.0–4.2 Å).

### Comparison of antimycin and ubiquinone binding positions; local conformational changes induced by antimycin

Disappointingly, the ubiquinone molecule in the crystals without antimycin (1PP9 and Y21) is much less well ordered than antimycin in 1PPJ. There is density in the position indicated for the ubiquinone ring by previous structures (1BCC and 1EZV), however, the shape is not well defined. It seems likely that the occupancy is significantly less than one, due to dissociation during the purification in detergent-containing, quinone-free buffers. Water or other molecules may have entered the unoccupied  $Q_i$  sites, resulting in the poorly defined density of the crystallographic average. Current experiments are aimed at maintaining a high quinone occupancy by purification in detergent micelles doped with ubiquinone.

There is no strong indication of asymmetric ubiquinone occupancy such as reported<sup>64,65</sup> for the yeast enzyme with one mole of cytochrome c bound per dimer: The peaks of the density

attributed to ubiquinone in monomers 1 and 2 were 3.0 and 2.1 $\sigma$  in 1PP9, but 2.6 and 2.8 $\sigma$  in Y21. The shapes were similar. Ubiquinone has been modeled into the density based on the previous structures, and refinement of the model did not lead to significant discrepancies from those structures. Thus, the results obtained superimposing Y21 below are essentially the same as would be obtained superimposing the yeast or chicken structures. Another bovine structure (1NTZ) presents a slightly shifted position for ubiquinone.

Figure 7 shows superposition of the  $Q_i$  sites of 1PPJ and Y21 based on a rigid core of cytochrome b, including the four-helix bundle<sup>†</sup>. The quinone ring does not superimpose with the aromatic salicylate ring of antimycin, rather it is centered on the carbonyl carbon of the amide group. Carbonyl oxygen O1 of the quinone is positioned near the phenolic OH oxygen of antimycin (0.63 Å) making the same H-bonds to Asp228 and water W3 as that atom makes. The other carbonyl oxygen, O4, extends toward His201, reaching farther than the carbonyl oxygen of the antimycin amide and

<sup>†</sup> The structure Y21 was chosen because its cell is most nearly isomorphous with 1PPJ, whereas 1PP9 has significantly different cell parameters. However, superimposing 1PP9, or for that matter the yeast or chicken structures, puts ubiquinone in essentially the same place.

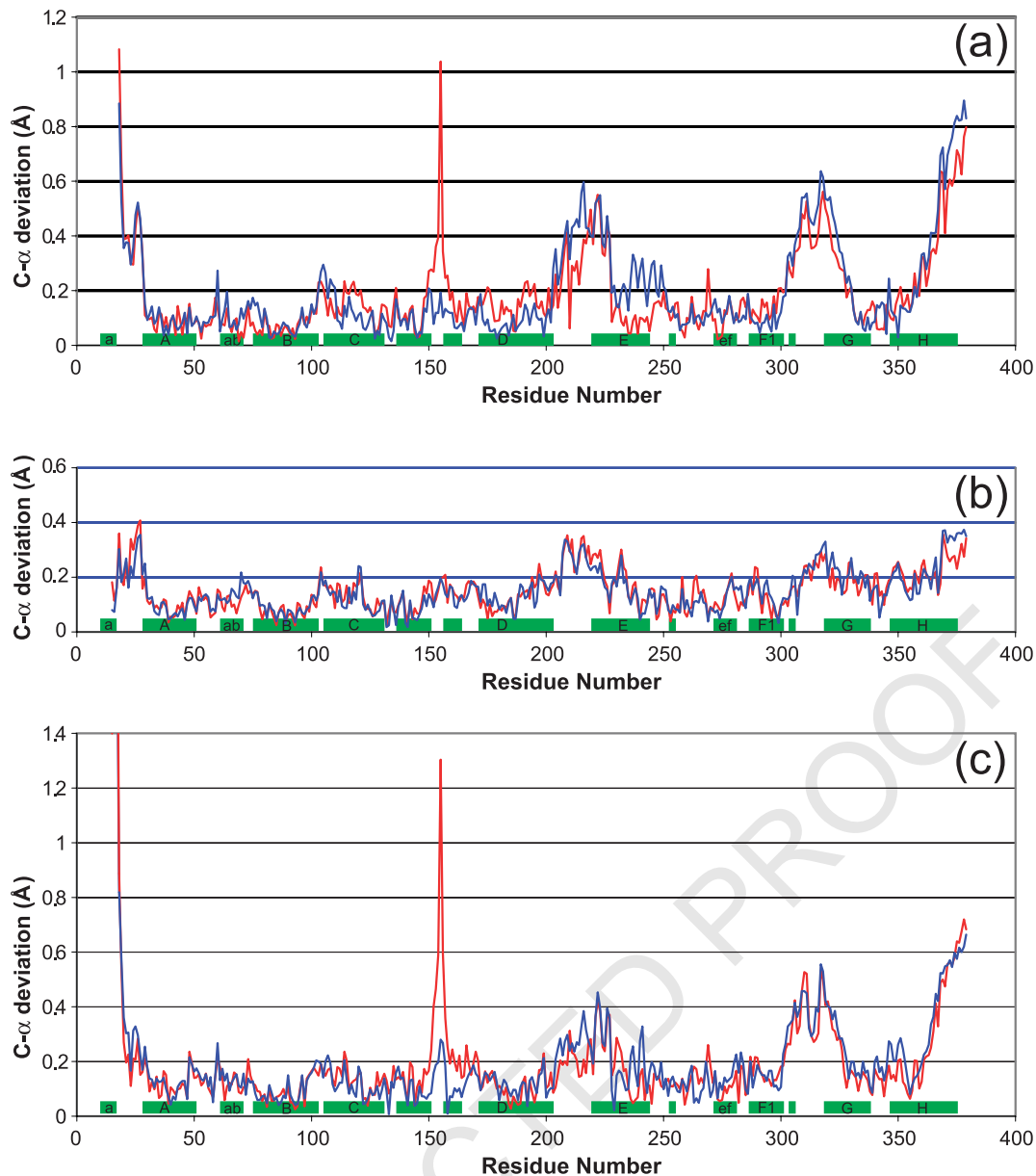


**Figure 8.** Flexibility in cytochrome b induced by antimycin and/or crystal packing forces. Various cytochrome b structures were aligned based on the relatively rigid core consisting of residues 32–51, 79–99, 113–145, 161–201, and 263–300. Deviations of C<sup>α</sup> position are plotted *versus* residue number for selected pairs of structures. For each pair the differences in chain C are shown in red while those for chain P are in blue. The green rectangles along the x axis indicate the position of helices in the sequence. PDB entries 1PP9 (without) and 1PPJ (with antimycin) are the structures featured here, while structure Y21 is from a crystal with cell parameters nearly identical with those of 1PPJ. Thus, comparison of cytochrome b from the same monomer between 1PPJ with Y21 (b) gives the best indication of antimycin-induced changes, while comparison of two monomers in the same crystal, or of 1PP9 with Y21 (c), should show only crystal-packing-induced changes. Comparison of 1PP9 with 1PPJ (a) superimposes both sets of changes.

making a direct H-bond (or a water-mediated H-bond in the yeast structures) with that residue.

There is surprisingly little rearrangement in the protein backbone and even side-chains surrounding antimycin, as compared with for example the rearrangement of protein around the Q<sub>o</sub> site upon binding inhibitors.<sup>23,66</sup> Gao *et al.*<sup>24</sup> also remarked on the structural rigidity of cytochrome b on antimycin binding, but reported significant conformational changes of cytochrome b residues Ser35, His201, Phe15, and Met194. Comparing structure 1PPJ with

1PP9 or Y21 (Figure 7) showed Ser35 to be identical and His201 not to have changed significantly. We see both conformations for Met194 in the presence or absence of antimycin. The side-chain of Phe15 is completely disordered in all three structures.

**Long-range conformational changes induced by antimycin binding and by different crystal packing forces**

As described in Introduction, there are several

**Table 5.** Relative motion of domains of cytochrome b between three crystals

	Chain C			Chain P		
	Angle (deg.)	Max disp	Atom	Angle (deg.)	Max disp	Atom
F <sub>2</sub> , G, H helices <i>versus</i> cytochrome b core						
1PP9 <i>versus</i> 1PPJ	1.392	0.8389	C378	1.169	0.6904	P378
1PPJ <i>versus</i> Y21	0.437	0.3072	C378	0.310	0.2654	P377
1PP9 <i>versus</i> Y21	0.960	0.5969	C378	0.944	0.5979	P378
E helix after 227 <i>versus</i> cytochrome b core						
1PP9 <i>versus</i> 1PPJ	0.927	0.3315	C245	0.503	0.1145	P245
1PPJ <i>versus</i> Y21	0.301	0.1486	C245	0.513	0.1814	P230
1PP9 <i>versus</i> Y21	0.859	0.2438	C245	0.349	0.1600	P228

reasons to believe that antimycin binding triggers a long-range conformational change in the  $bc_1$  complex. cursory comparison of the structures described here gives no indication of such a change: the differences between crystals with and without antimycin are smaller than differences between crystals with the same  $Q_o$ -site occupancy but different cell parameters, attributed to crystal packing distortions. The comprehensive comparison that would be required to put an upper limit on the magnitude of change that might be due to antimycin binding is beyond the scope of this work, however some preliminary quantitative comparisons will be described which indicate that the change must be quite small. The conformational changes observed are also of interest to indicate the modes of flexibility of the protein, whether due to crystal packing forces or inhibitor binding.

In order to look for conformational changes induced by antimycin binding, we compared C<sup>α</sup> positions of cytochrome b in structure 1PPJ with structures lacking antimycin (Figure 8 and Table 5). Structure 1PP9 lacks antimycin but has significantly different cell parameters (Table 1A) from 1PPJ, so differences may be due to different packing forces. A third structure of similar resolution (optical resolution 1.70) and lacking antimycin but with cell parameters similar to 1PPJ was compared to control for these changes.

In the structures compared here (all containing stigmatellin), a core domain of cytochrome b consisting of the four TMH of the four-helix bundle plus much of  $cd_1$ - $cd_2$ , the  $ef$ -linker, and the F helix before the kink at 300 ( $\alpha F1$ ) could be superimposed with rmsd 0.133 Å or below and maximum deviation 0.28 Å. The exact residues included in this core are listed in the legend to Figure 8, which shows the by-residue deviation, between 1PPJ (with antimycin) and two structures without antimycin, when cytochrome  $b$  is thus superimposed.

The N terminus and the  $de$  linker, both involved in the  $Q_i$  site, were significantly different between 1PPJ and 1PP9, while the  $ab$  and  $bc$  linkers showed minor deviations. The mobile region in the  $de$  loop actually extends into the N-terminal part of helix E, as far as residue Lys227. Although significant, these movements are very slight, as can be seen in Figure 7.

Helix E starting at 228 could be included in the core domain but gave a slight but perhaps significant increase in rms deviation between the C chains of 1PPJ and 1PP9 (but not between P chains). To test the hypothesis that the E helix transmits a conformational signal to the P side upon antimycin binding at the  $Q_i$  site, helix E was excluded from the core region used for superposition, and treated as a separate domain.

With the cytochrome b chains thus superimposed, distance between corresponding atoms in pairs of chains were plotted in Figure 8. Any large effect of antimycin should be seen as differences between 1PPJ (with antimycin) and 1PP9 or Y21, and not between 1PP9 and Y21 (both without antimycin).

Such by-residue plots of atom deviation are limited in sensitivity by the inherent noise in the structure, the estimated standard deviation for atom positions being 0.3–0.5 Å for these structures (Table 1B). If it is assumed that sections of protein move as rigid bodies, much smaller movements can be detected because positions of all the atoms in the body contribute to determining its position and the “jitter” in individual atomic positions averages out. We tested two domains for such rigid body movement relative to the core domain used for superposition. One was the helix F<sub>2</sub>+G+H region discussed below, which seems to be moving independently between 1PPJ and 1PP9, and the other was helix E, which shows significant deviations between these structures in the C chain (Figure 8(a)). To do this the operator best superimposing the domain in question was compared with the operator superimposing the core domain, giving an operator for the additional movement required to superimpose the domain in question after the core domain has been superimposed. This operator was then expressed as a rotation angle and as the largest movement of any atom in the domain upon application of the operator.

As a control to test the significances of the differences observed, the Y21 structure was re-solved twice starting with structures 1PPJ in one case and 1PP9 in the other. After positioning the models using the now-well-known intercrystal operators followed by rigid-body refinement and a few rounds of alternating positional minimization

and restrained atomic *B*-factor refinement, the entire cytochrome *b* backbone (excluding the disordered region before residue 20<sup>†</sup>) was superimposable with maximum deviation 0.16 Å and RMSD 0.04. This implies that the small differences observed in this region between 1PPJ and 1PP9 are within the radius of convergence of positional refinement, and thus reflect real differences in the data and not results of accidental differences in the history of model-building.

The results from the comparison of interdomain operators are listed in Table 5. The **G** and **H** helices together with helix **F** after the kink at residue 299 ( $\alpha$ F2) form a separate domain which is rotated significantly with respect to the core domain described above: a rotation of 1.3° with maximum C $\alpha$  displacement (at C378) of 0.81 Å in the case of C chains of 1PPJ and 1PP9). However, the differences correspond more to differences in cell parameters and which of the two monomers in the dimer is being compared than to the presence or absence of antimycin, suggesting they result from different packing forces rather than an antimycin-induced change. The largest changes are seen comparing 1PP9 and 1PPJ, which differ in both presence of antimycin and cell parameters. Comparing the Y21 structure with 1PP9 (difference in cell parameters) and with 1PPJ (presence or absence of antimycin), 1PP9 shows the greatest movement of the **F**<sub>2</sub>**GH** domain in both C and P chains, and the largest movement in helix **E** for chain C. While movement of the **E** helix in chain P was largest in 1PPJ, that movement was a barely significant 0.51° rotation with maximal atomic displacement of 0.18 Å. This would appear to limit any antimycin-induced, long-range, static, conformational changes to a very subtle effect, at least in the presence of stigmatellin.

### Ramachandran outliers

It is normal for well-refined structures even at high resolution to have 0.1–0.5% of residues in the “Forbidden” zone of the Ramachandran plot. However, a Ramachandran outlier can also be an indication of a mis-built residue. Therefore we have examined the outliers in the two structures presented here to see how well the conformation presented is supported by the density.

Tyr155 of cytochrome *b* is a particularly interesting outlier that is well supported by the density. In

<sup>†</sup> The N terminus of cytochrome *b* up to residue 20 is modeled differently in 1PP9 and 1PPJ, to the extent that manual rebuilding would be required for convergence when refined against the same data. Density is not very clear here and it seems likely that multiple conformations exist for all three structures. This region was modeled differently in the bovine cytochrome *bc*<sub>1</sub> structures from Uppsala (1BE3, 1BGY) as compared to those from Bethesda (e.g. 1L0L). The possibility has been raised<sup>77</sup> that the N terminus including  $\alpha$ -a helix serves to transmit a conformational signal between **Q**<sub>i</sub> sites of the two monomers.

bacterial *bc*<sub>1</sub> complexes, there are two conserved glycine residues in the turn between helices **cd**<sub>1</sub> and **cd**<sub>2</sub>, corresponding to positions 155 and 157 in the bovine sequence. Gly157 is also conserved in the mitochondrial complexes, but surprisingly 155 tends to be an aromatic tyrosine in most vertebrates, phenylalanine in yeast. However the backbone phi, psi values for this residue are 66° to 68° and –39° to –42° in the bovine structures and 76.6°, –75.0° in the yeast structure. These values lie outside the allowed region on the Ramachandran plot for any residue but glycine. Thus, a mitochondrial progenitor has placed an aromatic at a position in the fold where only glycine could be accommodated readily, and this strained aromatic has been preserved through evolution. We will not speculate about the function, but note that the  $\alpha$ cd<sub>1</sub>-cd<sub>2</sub> hairpin helix forms part of the **Q**<sub>o</sub> site, and movement of this helix in response to **Q**<sub>o</sub>-site occupancy or ISP position has been reported.<sup>23,66</sup>

The residue corresponding to Tyr155 is also a Ramachandran outlier in all available structures of the chicken or yeast *bc*<sub>1</sub> complex, and in the bovine complex in tetragonal crystals (e.g. 1L0L). Outlier status is avoided in structures 1BE3 and 1BGY by flipping the plane of the preceding peptide (154–155) relative to all other structures, however this arrangement of the backbone is incompatible with the density in the crystals reported here. The backbone density for this residue is quite strong and unambiguous, however the density on the ring and OH has a peculiar shape. This side-chain sticks out into the solvent from the turn of the **cd**<sub>1</sub>-**cd**<sub>2</sub> hairpin and makes no contacts with the rest of the protein, so it is not surprising if it is not well ordered. In chain P, the tip of the side-chain of Tyr155 makes a crystal contact (with chain B of a symmetry-related dimer). This contact varies with cell volume, resulting in the spike at residue 155 in Figure 8(a) and (c).

Residue Ala171 in chain B (“core II”) also falls in the disallowed region of the Ramachandran plot. This is in a 3–10 helical turn at the end of helix  $\alpha$ D||. The electron density leaves little doubt as to the positions of the atoms, so we believe this also is a real outlier. It is an outlier in the yeast (1P84) and tetragonal bovine (1L0L) structures as well, but not in 1BGY, again as a result of flipping the peptide plane (B170–B171) in a way which is inconsistent with the density in our structures.

Residue Met71 in the “tether” region of the iron-sulfur protein differs in the two monomers. The conformation modeled in the first monomer (chain E) is an outlier in the structure deposited for 1PPJ (with antimycin), but not in 1PP9 or the Y21 structure, or in chain R of any structure. This residue appears to have several conformations and is not very well ordered. It is likely subjected to considerable strain in some positions of the ISP extrinsic domain, which could provide the energy for an unfavorable backbone conformation. This dynamic linker region is worthy of further study to decide if it is really an outlier in some of its

2269 conformations, and to better define the different  
2270 conformations.

2271 The other two Ramachandran outliers are found  
2272 in poorly defined regions (A223,224 in the inter-  
2273 domain linker of the largest subunit) and probably  
2274 represent errors in the model.

2275  
2276  
2277

## 2277 Discussion

2278 A number of features of the *bc*<sub>1</sub> complex revealed  
2279 by the presented structures and not discerned in  
2280 previous structures suggests that this is the most  
2281 accurate structure of the *bc*<sub>1</sub> complex available. In  
2282 particular, the binding mode of the inhibitor  
2283 antimycin is defined to a high level of accuracy.  
2284 The new structure is consistent with results of  
2285 structure–activity relationship studies, however it  
2286 does not support one of the conclusions from those  
2287 studies: that the intramolecular hydrogen bond  
2288 between phenolic OH and carbonyl O described for  
2289 the molecule in solution<sup>38</sup> and in the small-molecule  
2290 crystal<sup>42</sup> is important for binding and inhibitory  
2291 activity. On the contrary, the bound molecule has  
2292 the carbonyl oxygen facing His201 with a long,  
2293 weak, or water-mediated hydrogen bond while the  
2294 amide nitrogen H-bonds to the phenolic hydroxyl  
2295 oxygen. This is quite understandable because the  
2296 phenolic OH group is H-bonding to aspartate and is  
2297 likely to be the donor in that interaction. This would  
2298 make an H-bond to the carbonyl oxygen impossible,  
2299 as that atom can only be an H-bond acceptor. The  
2300 amide nitrogen, on the other hand, has one proton  
2301 that would be available for H-bond donation. Such  
2302 a rearrangement of the H-bonding pattern upon  
2303 binding is not surprising, in fact the possibility was  
2304 suggested in the small-molecule structure report.<sup>42</sup>  
2305 The importance of the intramolecular H-bond was  
2306 inferred from the fact that an antimycin analog in  
2307 which the amide is separated from the salicylate  
2308 benzene ring by an extra carbon (compound B of  
2309 Miyoshi *et al.*<sup>38</sup>) and thus could not form the  
2310 H-bond, was 10<sup>4</sup>-fold less potent than an analogue  
2311 with the amide directly connected as in antimycin.  
2312 However, this compound would be equally unable  
2313 to form the intramolecular H-bond between amide  
2314 nitrogen and phenolic oxygen that we observe in  
2315 the bound inhibitor, so these experimental results  
2316 are consistent with our structure. In fact it could be  
2317 said that our structure supports the conclusion of  
2318 that study regarding the importance of an internal  
2319 H-bond between phenolic oxygen and the amide,  
2320 but those experiments gave no hint that the amide is  
2321 flipped; and the amide N, rather than O, is involved  
2322 in the H-bond.

2323 The structure of bound antimycin and the  
2324 surrounding protein presented here differs in  
2325 some significant details from that of the structure  
2326 1NTK.<sup>24</sup> Most importantly, the conformation of  
2327 antimycin in the binding site is different. While  
2328 both structures agree that the dilactone and  
2329 formylaminosalicylate rings are rotated relative to  
2330 each other as compared to the small-molecule  
2331

2332 structure, 1NTK keeps the dihedral between the  
2333 amide moiety and the FSA fixed, preserving the  
2334 intramolecular H-bond between the phenolic OH  
2335 and the amide O. In 1PPJ there is 180° rotation about  
2336 this dihedral relative to the small-molecule struc-  
2337 ture, breaking the intramolecular bond and forming  
2338 a new one between the amide NH group and the  
2339 phenolic O.

2340 In addition two key residues Ser35 and Lys227  
2341 have their side-chains modeled differently in the  
2342 two structures, resulting in different roles for these  
2343 residues in antimycin binding. Gao *et al.*<sup>24</sup> report  
2344 from structure 1NTK that Ser35 forms H-bonds  
2345 with the amide carbonyl O and a carbonyl O of the  
2346 dilactone ring. In 1PPJ Ser35 is in the most stable  
2347 rotamer, facing away from antimycin (Figure 5(b))  
2348 and H-bonds with two water molecules (W3, W2)  
2349 and the carbonyl oxygen of residue 32, but makes  
2350 no direct H-bond to antimycin. If it were changed to  
2351 rotamer 2<sup>c</sup> it would be positioned to H-bond  
2352 the carbonyl oxygen of the threonine moiety of the  
2353 dilactone, as in the model of Gao *et al.* However the  
2354 electron density (Figure 5(a)) gives no indication of  
2355 Ser35 in rotamer 2, even at partial occupancy. On  
2356 the contrary, as described above W3 mediates an  
2357 H-bond between Ser35 and the phenolic OH of  
2358 antimycin. Likewise Lys227N<sup>c</sup> makes a direct bond  
2359 to the formylamino oxygen of antimycin in 1NTK,  
2360 but in 1PPJ these atoms are 5.2 Å apart and ordered  
2361 water W1 binds between them (Figure 5(b) and 6).  
2362 Neither structure has Lys227 in one of the five most  
2363 common rotamers, however in 1PPJ it is in rotamer  
2364 26 (3% frequency) of the more extensive rotamer  
2365 library described by Lovell *et al.*<sup>67</sup>

2366 Whenever different results are obtained from two  
2367 different crystal forms of the same protein under  
2368 different conditions, it has to be asked whether the  
2369 different results correctly represent two different  
2370 states of the protein (possibly corresponding to  
2371 different steps along a reaction pathway) or  
2372 whether the feature is actually invariant and one  
2373 of the structures is in error. In the case of the  
2374 orientation of the antimycin amide group, it seems  
2375 unlikely that both binding modes are possible.  
2376 Unfortunately, supporting data (structure factors)  
2377 are not available for the 1NTK structure, which  
2378 makes it impossible to test whether the data would  
2379 have been equally consistent with our current  
2380 model. However the density depicted in the  
2381 stereodiagram of Figure 2(A) of Gao *et al.*<sup>24</sup>  
2382 appears consistent with our structure, having an  
2383 unaccounted-for protrusion about where we put the  
2384 carbonyl oxygen, and having the modeled carbonyl  
2385 oxygen at the edge of contoured density with no  
2386 surrounding protrusion of the density.

2387 While we want to emphasize that the structure of  
2388 antimycin in 1PPJ is based on the electron density  
2389 from X-ray diffraction by a crystal and not on  
2390 chemical considerations or structure–activity  
2391 relationships, the flipping of the salicylate amide  
2392 moiety relative to the small-molecule structure seen  
2393 here nicely explains why compound **D** of Miyoshi  
2394 *et al.*,<sup>38</sup> which is methylated on the amide N, is a

2395 poor inhibitor despite still having the internal  
2396 H-bond (albeit weaker) between phenolic OH and  
2397 carbonyl oxygen in solution. The amide of a  
2398 secondary amine cannot be a hydrogen-bond  
2399 donor, so the intramolecular H-bond that we see  
2400 between phenolic OH and amide N cannot form,  
2401 and the methyl group would clash with the  
2402 phenolic OH preventing the molecule from taking  
2403 this conformation. The explanation is less obvious  
2404 with the structure presented in 1NTK, as the amide  
2405 nitrogen is oriented toward a spacious part of the  
2406 pocket containing only water molecules that might  
2407 be expected to be displaceable (although methyl-  
2408 ation would prevent H-bonding with the water).

2409 As for the discrepancies regarding the roles of  
2410 Ser35 and Lys128, it seems more possible that the  
2411 different rotamers observed in the current 1PPJ  
2412 structure as opposed to 1NTK represent different  
2413 states depending on pH or ionic strength. However,  
2414 the failure of that structure to correctly orient the  
2415 amide linkage weakens the argument for different  
2416 conformations of these residues. Since electron  
2417 density was not shown supporting the modeled  
2418 rotamers, and data are not available for indepen-  
2419 dent evaluation, we hesitate to propose alternate  
2420 conformations for these residues at this time.

2421 Ser35 is not required for antimycin binding, as  
2422 *Rhodobacter* and *Paracoccus*, which have Val or Ile  
2423 here, are inhibited by antimycin. However  
2424 *Rhodospirillum rubrum* has Ser as in mitochondria,  
2425 and is more sensitive (in whole cells) than  
2426 *Rhodobacter* (F. Daldal, personal communication).  
2427 Schnauffer *et al.*<sup>68</sup> found that mutation of Ser35 to Ile  
2428 led to antimycin resistance in *L. tarentolae*. However  
2429 the effect of Ser35Ile substitution might be expected  
2430 due to steric effects, and is not necessarily indicative  
2431 of a role of this residue in H-bonding to antimycin  
2432 or stabilizing the water molecules involved in  
2433 antimycin binding.

2434 Despite evidence summarized in the introduction  
2435 for a long-range conformational change induced by  
2436 antimycin binding, no indication of such a change  
2437 has been reported from the previous X-ray struc-  
2438 tures. Our analysis of the present structures also  
2439 gives no indication of such a change, suggesting it  
2440 must be a rather subtle change if it exists at all.  
2441 Much of the evidence for a conformational change is  
2442 circumstantial, and perhaps amenable to alternative  
2443 explanations. For example the effect of antimycin on  
2444 the stability in bile salts may involve strong binding  
2445 interactions between the inhibitor and the protein  
2446 serving to hold together the different parts of the  
2447 sequence contributing to the binding site more  
2448 strongly than they would be held together in the  
2449 absence of the inhibitor, perhaps tying down a loose  
2450 end to prevent some kind of "unraveling" which  
2451 may initiate the cleavage reaction.

2452 Antimycin may affect conformational dynamics  
2453 of the protein in solution or embedded in the lipid  
2454 bilayer, allowing or preventing the visitation of  
2455 certain conformational states while not affecting the  
2456 resting state that we see in the crystal, and these  
2457 transient states may be responsible for the observed

2458 effects. It must also be remembered that all  
2459 structures being compared here have stigmatellin  
2460 at the *Q*<sub>o</sub> site, and it is possible that this tight-  
2461 binding inhibitor locks the conformation of The *Q*<sub>o</sub>  
2462 region and prevents conformational changes that  
2463 would otherwise have been induced by antimycin.  
2464 A similar comparison made with the chicken *bc*<sub>1</sub>  
2465 crystals in the absence of stigmatellin did not show  
2466 any clear antimycin-induced change,<sup>23</sup> but the  
2467 resolution was lower and refinement not very  
2468 complete at that time.

## 2470 Materials and Methods

2471 Bovine hearts were obtained from a slaughterhouse or  
2472 meat market and either used fresh or stored at -20 °C or  
2473 below before use in the mitochondrial preparation. "Sol-  
2474 grade" dodecyl β-D-maltopyranoside (DM) and  
2475 "anagrade" hexyl-β-D-glucopyranoside (HG) were pur-  
2476 chased from Anatrace. Stigmatellin and polyethylene  
2477 glycol (PEG) were from Fluka. Crystallization screen kits  
2478 mentioned below, as well as cryocrystallography  
2479 supplies, were from Hampton Research.

2480 Mitochondrial protein was determined by the Lowry  
2481 method<sup>69</sup> with bovine serum albumin as a standard.  
2482 Cytochrome *bc*<sub>1</sub> concentration was determined from the  
2483 difference in absorbance of the dithionite-reduced sample  
2484 at 562 versus 600 nm, for which an extinction coefficient  
2485 for the bovine enzyme of 70 cm<sup>-1</sup> mM<sup>-1</sup> (E. Berry,  
2486 unpublished results; based on pyridine hemochrome  
2487 analysis) was used.

## 2489 Protein purification

2490 Purification was as described,<sup>70</sup> involving solu-  
2491 bilization of mitochondria with 1.0 g DM per gram  
2492 protein, anion exchange chromatography on DEAE  
2493 Sepharose CL6B with a gradient from 260 mM to  
2494 500 mM NaCl (in 50 mM KPi buffer (pH 7.5), 0.5 mM  
2495 EDTA, 0.1 g/l DM) and size-exclusion chromatography  
2496 on Sepharose CL-6B in "sizing buffer" (20 mM K-Mops  
2497 (pH 7.2), 100 mM NaCl, 0.5 mM EDTA, 0.1 g/l DM).  
2498 Pooled fractions from the last column were adjusted to  
2499 5 μM cytochrome *bc*<sub>1</sub> by ultrafiltration or dilution in the  
2500 same buffer. Stigmatellin and Antimycin A were added to  
2501 10 μM (twofold molar excess) from 10 mM and 15 mM  
2502 alcoholic stock solutions.

2503 Before setting up crystallization droplets a final step  
2504 (PEG fractionation) was carried out in which the  
2505 inhibitor-loaded *bc*<sub>1</sub> complex was mixed with successive  
2506 portions of a precipitant solution containing 100 mM  
2507 K-Mes (pH 6.4), 100 g/l PEG 4k, and 0.5 mM EDTA. This  
2508 procedure clearly separates two populations, a minor  
2509 fraction ("aggregated material") which usually precipi-  
2510 tates at around 0.3 volumes of precipitant and contains all  
2511 of the contaminating cytochrome oxidase (present as  
2512 supercomplex or micelles containing two separate  
2513 complexes, and incompletely separated by the size-  
2514 exclusion column) from the major fraction which usually  
2515 does not begin to precipitate until more than 0.6 volumes  
2516 have been added. In the case of the antimycin-containing  
2517 crystal, material precipitating between 0.29 and 0.76  
2518 volumes of precipitant was collected by centrifugation  
2519 and redissolved in several times the original volume of  
2520 the above-mentioned sizing buffer. To reduce NaCl and  
2521 residual PEG from precrystallization, the buffer was

exchanged by several cycles of dilution in final buffer (20 mM Tris-HCl (pH 7.5), 0.5 mM EDTA, 1 g/l UDM) and ultrafiltration on Amicon YM-100 membrane. It is difficult to dissolve the PEG-fractionation pellet directly in a small volume of final buffer- perhaps due to residual PEG it is necessary to have a higher ionic strength, provided by NaCl in the sizing buffer.

**Crystallization**

Crystallization was by sitting-drop vapor diffusion. Protein in the final buffer described above was mixed with 0.15 volume of 2.5 M HG, and then one volume (usually 10 μl) of this detergent-supplemented protein was mixed with 0.9 volume of major precipitant and 0.1 volume of minor precipitant/additive. The major precipitant consisted of 60 g/l PEG-3350, 100 g/l glycerol, 100 mM Na-cacodylate (pH 6.7), 20 mM MgCl<sub>2</sub>, and 3 mM NaN<sub>3</sub>, and the minor precipitant/additive was Hampton Research's "Screen II #31", consisting of 200 g/l Jeffamine M600 in 0.1 M Hepes (pH 7.5).

We calculate the final pH to be about 6.86, ignoring buffering by the protein itself. The ionic strength is 72 mM before vapor diffusion. The droplets were allowed to equilibrate by vapor diffusion against a reservoir containing the major precipitant.

**Data collection**

The crystals were mounted in a nylon loop on a magnetic pin (Hampton Research) and flash-cooled in liquid nitrogen for cryogenic data collection. The diffraction limit and the cell parameters were highly variable, and in some cases warming the crystal to room temperature for one to two minutes and refreezing in the cold stream improved the diffraction dramatically. This seems to be related to the extent of dehydration of the crystals, and we are currently working on a way to optimize the diffraction by systematic dehydration.

The crystal from which structure 1PPJ was obtained was mounted in a loop and dipped in a mixture containing equal parts of the mother liquor and cryoprotectant (250 ml/l glycerol, 120 g/l PEG 4k, 10 mM K-Mes (pH 6.7), 3 mM Azide) before freezing in liquid nitrogen. After a preliminary exposure revealed diffraction to 4 Å and space group *P*2<sub>1</sub>2<sub>1</sub>2<sub>1</sub> with cell parameters 152 × 178 × 227, the pin was removed from the cold stream and set, base down, at room temperature, so the crystal in the loop was dehydrated by the downdraft produced by the cold copper pin. After three minutes, the pin was returned to the cold stream for data collection, now with resolution limit 2.0 Å and cell parameters 128, 169, 232.

The crystal for structure 1PP9 (without antimycin) was not intentionally dehydrated, however it was one of only two crystals diffracting to around 2 Å from about 40 that were mounted from the same well. It is likely that these two crystals were exposed to air longer than the others before freezing. The cell parameters for 1PP9 are somewhat intermediate between the before and after parameters for 1PPJ, suggesting it is less dehydrated. The other crystal from that well diffracting to 2.0 Å had essentially the same cell parameters as 1PPJ. This is the crystal Y21, mentioned in the discussion of antimycin-induced structural changes.

Diffraction patterns were collected in 0.5° rotations.

Even for the best diffracting crystals, the mosaic spread was large (1.0–1.5°). In order to reduce the data to 2.0 Å without excessive overlap, it was necessary to assume a lower mosaic spread (0.6°) during spot integration. This results in sampling spot intensity near the maximum of the rocking curve ("profile peak sampling") but ignores tails of the measured reflection's rocking curve as well as overlap from tails of neighboring spots in reciprocal space. This together with radiation decay described below contributes to the higher than usual *R*<sub>merge</sub> and *R*<sub>sym</sub> values for these datasets.

Both crystals used in this work were rod-shaped, with dimensions ~0.2 × 0.2 × 1.5 mm<sup>3</sup>. This allowed collecting several different datasets from each crystal, at different positions along the long axis of the crystal. It was later determined that significant radiation damage occurred during data collection as indicated by increasing *B*-factor. In the case of the antimycin-containing crystal (1PPJ), the final dataset was constructed by merging early data from each individual dataset, with a cutoff when the *B*-factor for scaling against a particular reference was more than 15 Å<sup>2</sup> greater than that for the first exposures. The measurements from these selected frames from each data collection were individually scaled and merged in scalepack.<sup>71</sup> The resulting incomplete datasets were merged together using scalepack to make the final dataset. The statistic *R*<sub>merge</sub> in Table 1 and in the PDB file header refers to the *R*-merge obtained at this second merging step. For structure 1PP9 data from a single collection was used and *R*<sub>merge</sub> in Table 1 (*R*<sub>sym</sub> in the PDB entry) refers to the initial merging of frames within the dataset.

To prepare for cross-validated (cv) refinement<sup>72</sup> a test set of reflections ("Free-R flags") was chosen from an ideally generated complete dataset to 1.8 Å, randomly selecting 5% of the reflections. This set of Free-R flags was used with every dataset from this crystal form to avoid biasing the cross-validation.

**Structure determination**

*Phasing*

The first (low resolution) dataset from a crystal of this new orthorhombic form was solved by molecular replacement using PDB entry 1BE3 as model. The iron-sulfur proteins were repositioned as in entry 2BCC, and several regions that were observed not to fit the 2*F*<sub>o</sub> - *F*<sub>c</sub> density map were rebuilt. As successively higher resolution datasets were collected, they were phased by molecular replacement using the best available previous structure from the same crystal form. Variation in cell parameters made rigid body refinement of the previous structure against the new data unreliable for positioning the molecule in the cell.

For each crystal, the model was refined by cycles of manual rebuilding using the graphics program O<sup>73</sup> alternating with rigid body, multi-rigid-body, positional, and restrained atomic *B*-factor refinement in CNS.<sup>74</sup> When significant improvement was achieved in one crystal, the appropriate changes were transferred to the other crystals by refining the improved model to convergence against the other datasets, comparing atomic positions with the previous models for those datasets, and examining the differences in the density to decide which model was appropriate on a crystal-by-crystal and residue-by-residue basis.

2647 *Non-crystallographic symmetry*

2648 The crystal contains a dimer of the bc<sub>1</sub> complex in the  
 2649 asymmetric unit. Initially non-crystallographic symmetry  
 2650 restraints were used for all protein atoms. During  
 2651 rebuilding, to fit the electron density it became clear  
 2652 that certain residues did not obey NCS, and the restraints  
 2653 were released for those residues. For a while, NCS  
 2654 restraints were eliminated, and the two monomers were  
 2655 refined and rebuilt independently. The resulting structure  
 2656 was examined to locate areas that seemed to violate NCS,  
 2657 and restraints were re-applied everywhere else. The  
 2658 remaining NCS violations were examined to determine  
 2659 whether the electron density supported the violation. If  
 2660 not, the residue was rebuilt in both monomers to be  
 2661 consistent with NCS and the restraint was re-imposed. If  
 2662 the NCS violation appeared real, the surrounding was  
 2663 examined for explanations in the form of crystal contacts.  
 2664 Except in the case of clear NCS violations, application of  
 2665 NCS restraints invariably improved the R-free statistic. It  
 2666 is not known, however to what extent this is due to  
 2667 improvement in the ratio of (data+restraints) to par-  
 2668 ameters, and to what extent to communication between  
 2669 the test and working sets of reflections (bias) due to the  
 2670 NCS relationship.

2671 In addition to specific violations of NCS, subtle  
 2672 distortions of the protein between the two monomers  
 2673 were present, presumably due to intrinsic flexibility of  
 2674 the protein and the different packing forces. To allow for this  
 2675 flexibility without greatly increasing the number of  
 2676 parameters being fit, the NCS-restrained residues were  
 2677 divided into about 49 NCS groups each of which was  
 2678 allowed its own NCS operator.

2678 *Solvent*

2679 Water molecules were added with the water\_pick  
 2680 program of CNS, and refreshed periodically by removal  
 2681 of water molecules flagged by whatcheck as too far from  
 2682 protein and picking of new water molecules. As the  
 2683 density improved, some of the solvent molecules took on  
 2684 distinct oblong or trigonal shapes, and some of these were  
 2685 modeled as oxygen or azide and glycerol, respectively.  
 2686 Phospholipid and detergent molecules appeared in  
 2687 varying states of disorder, and some of the best-defined  
 2688 have been modeled.

2690 *Validation*

2691 The refined structures were subjected to validation  
 2692 using PROCHECK,<sup>50</sup> SFCHECK<sup>48</sup> and whatcheck.<sup>75</sup>  
 2693 Residues flagged as unusual were examined and in  
 2694 many cases rebuilt, then the refinement was repeated  
 2695 before testing again. ARP/wARP version 6.0 was used to  
 2696 eliminate model bias and confirm the well-determined  
 2697 parts of the structure by automated rebuilding from free  
 2698 atoms refined by the ARP/wARP<sup>76</sup> process “automated  
 2699 model building starting from existing model”. ARP/  
 2700 wARP was able to trace the protein in as few as 53 chains  
 2701 containing over 3700 residues, as compared to 20 chains  
 2702 containing ~4020 residues in the final models.

2703 When these steps ceased to yield further improvement,  
 2704 the model was saved and then submitted to a final round  
 2705 of non-cross-validated refinement (positional and  
 2706 B-individual) using all the data, with all parameters the  
 2707 same as during the final cv refinement. No manual  
 2708 adjustment was performed on the final refined structure.  
 2709 Refinement statistics for deposition were obtained by the  
 “xtal\_pdbsubmission” routine of CNS using both the final

cv-refined structure and the final structure refined against  
 all the data. The coordinates of the latter structure and the  
 data used in refinement were deposited in the PDB.

**Protein Data Bank accession number**

Structure factors and coordinates have been submitted  
 to the Protein Data Bank under the accession numbers  
 1PP9 (without) and 1PPJ (with antimycin). The structure  
 referred to as Y21 is being deposited with accession  
 number 1???.  


---


---

**Acknowledgements**

We thank Antony R. Crofts, Patrick Crowley,  
 Fevzi Daldal, Chris Earnshaw, Hideto Miyoshi,  
 Graham Sexton, Bernard L. Trumpower, and  
 Ya-Jun Zheng for helpful discussions during the  
 course of this work and/or reading the manuscript  
 and providing valuable suggestions. This work was  
 supported by NIH research grants DK44842 from  
 NIDDK and by GM62563 from NIGMS. Lawrence  
 Berkeley National Lab (LBNL) is operated by the  
 Department of Energy, contract DE-AC03-  
 76SF00098 to the University of California.

Diffraction data were collected at the Advanced  
 Light Source (ALS) at LBNL and at the Stanford  
 Synchrotron Radiation Laboratory (SSRL), which is  
 operated by the Department of Energy, Office of  
 Basic Energy Sciences. The SSRL Biotechnology  
 Program is supported by the National Institutes of  
 Health, National Center for Research Resources,  
 Biomedical Technology Program, and by the  
 Department of Energy, Office of Biological and  
 Environmental Research. We thank Henry Belamy,  
 Nick Sauter, Aina Cohen, and Dan Harrington at  
 SSRL, and Keith Henderson and Corie Ralston at  
 the ALS, for help with data collection; and Nick  
 Sauter at LBNL for advice on data processing. The  
 PDB entries 1PP9 and 1PPJ were processed by Shri  
 Jain and Rose Oughtred of RCSB. The crystals  
 leading to structures 1PP9 and Y21 were grown by  
 Mr Yusef Collins, at that time supported by a  
 supplement to NIH grant GM62563.

**Supplementary Data**

Supplementary data associated with this article  
 can be found at [10.1016/j.jmb.2005.05.053](https://doi.org/10.1016/j.jmb.2005.05.053)

**References**

1. Mitchell, P. (1976). Possible molecular mechanisms of the protonmotive function of cytochrome systems. *J. Theor. Biol.* **62**, 327–367.
2. Crofts, A. R. & Meinhardt, S. W. (1982). A Q-cycle mechanism for the cyclic electron-transfer chain of Rhodospseudomonas sphaeroides. *Biochem. Soc. Trans.* **10**, 201–203.

2710  
2711  
2712  
2713  
2714  
2715  
2716  
2717  
2718  
2719  
2720  
2721  
2722  
2723  
2724  
2725  
2726  
2727  
2728  
2729  
2730  
2731  
2732  
2733  
2734  
2735  
2736  
2737  
2738  
2739  
2740  
2741  
2742  
2743  
2744  
2745  
2746  
2747  
2748  
2749  
2750  
2751  
2752  
2753  
2754  
2755  
2756  
2757  
2758  
2759  
2760  
2761  
2762  
2763  
2764  
2765  
2766  
2767  
2768  
2769  
2770  
2771  
2772

2773 3. Mitchell, P. (1974). A chemiosmotic molecular  
2774 mechanism for proton-translocating adenosine tri-  
2775 phosphatases. *FEBS Letters*, **43**, 189–194.

2776 4. Trumpower, B. L. (1976). Evidence for a protonmotive  
2777 Q cycle mechanism of electron transfer through the  
2778 cytochrome b-c<sub>1</sub> complex. *Biochem. Biophys. Res.*  
2779 *Commun.* **70**, 73–80.

2780 5. Slater, E. C. (1973). The mechanism of action of the  
2781 respiratory inhibitor, antimycin. *Biochim. Biophys.*  
2782 *Acta*, **301**, 129–154.

2783 6. Berden, J. A. & Slater, E. C. (1972). The allosteric  
2784 binding of antimycin to cytochrome b in the  
2785 mitochondrial membrane. *Biochim. Biophys. Acta*,  
2786 **256**, 199–215.

2787 7. Deul, D. H. & Thorn, M. B. (1962). Effects of 2,3-  
2788 dimercaptopropanol and antimycin on absorption  
2789 spectra of heart-muscle preparations. *Biochim.*  
2790 *Biophys. Acta*, **59**, 426–436.

2791 8. Chance, B. (1958). The kinetics and inhibition of  
2792 cytochrome components of the succinic oxidase  
2793 system. III. Cytochrome b. *J. Biol. Chem.* **233**,  
2794 1223–1229.

2795 9. Trumpower, B. L. & Katki, A. (1975). Controlled  
2796 reduction of cytochrome b in succinate-cytochrome c  
2797 reductase complex by succinate in the presence of  
2798 ascorbate and antimycin. *Biochem. Biophys. Res.*  
2799 *Commun.* **65**, 16–23.

2800 10. Wikstrom, M. K. & Berden, J. A. (1972). Oxidoreduc-  
2801 tion of cytochrome b in the presence of antimycin.  
2802 *Biochim. Biophys. Acta*, **283**, 403–420.

2803 11. Siedow, J. N., Power, S., de la Rosa, F. F. & Palmer, G.  
2804 (1978). The preparation and characterization of highly  
2805 purified, enzymically active complex III from baker's  
2806 yeast. *J. Biol. Chem.* **253**, 2392–2399.

2807 12. Yu, C. A., Nagaoka, S., Yu, L. & King, T. E. (1978).  
2808 Evidence for the existence of a ubiquinone protein  
2809 and its radical in the cytochromes b and c<sub>1</sub> region in  
2810 the mitochondrial electron transport chain. *Biochem.*  
2811 *Biophys. Res. Commun.* **82**, 1070–1078.

2812 13. Rieske, J. S., Baum, H., Stoner, C. D. & Lipton, S. H.  
2813 (1967). On the antimycin-sensitive cleavage of  
2814 complex 3 of the mitochondrial respiratory chain.  
2815 *J. Biol. Chem.* **242**, 4854–4866.

2816 14. Van Ark, G. & Berden, J. A. (1977). Binding of HQNO  
2817 to beef-heart sub-mitochondrial particles. *Biochim.*  
2818 *Biophys. Acta*, **459**, 119–127.

2819 15. Baum, H., Rieske, J. S., Silman, H. I. & Lipton, S. H.  
2820 (1967). On the mechanism of electron transfer in  
2821 complex III of the electron transfer chain. *Proc. Natl*  
2822 *Acad. Sci. USA*, **57**, 798–805.

2823 16. Rieske, J. S. (1980). Inhibitors of respiration at energy-  
2824 coupling site 2 of the respiratory chain. *Pharmacol.*  
2825 *Ther.* **11**, 415–450.

2826 17. Valkova-Valchanova, M., Darrouzet, E., Moomaw,  
2827 C. R., Slaughter, C. A. & Daldal, F. (2000). Proteolytic  
2828 cleavage of the Fe-S subunit hinge region of  
2829 Rhodobacter capsulatus bc<sub>1</sub> complex: effects of  
2830 inhibitors and mutations. *Biochemistry*, **39**,  
2831 15484–15492.

2832 18. Covian, R., Gutierrez-Cirlos, E. B. & Trumpower, B. L.  
2833 (2004). Anti-cooperative oxidation of ubiquinol by the  
2834 yeast cytochrome bc<sub>1</sub> complex. *J. Biol. Chem.* **279**,  
2835 15040–15049.

2836 19. Brandt, U. & von Jagow, G. (1991). Analysis of  
2837 inhibitor binding to the mitochondrial cytochrome c  
2838 reductase by fluorescence quench titration. Evidence  
2839 for a catalytic switch at the Q<sub>o</sub> center. *Eur. J. Biochem.*  
2840 **195**, 163–170.

2841 20. Zhang, Z., Huang, L., Shulmeister, V. M., Chi, Y. I.,  
2842 Kim, K. K., Hung, L. W. *et al.* (1998). Electron transfer  
2843 by domain movement in cytochrome bc<sub>1</sub>. *Nature*, **392**,  
2844 677–684.

2845 21. Brandt, U. (1998). The chemistry and mechanics of  
2846 ubihydroquinone oxidation at center P (Q<sub>o</sub>) of the  
2847 cytochrome bc<sub>1</sub> complex. *Biochim. Biophys. Acta*, **1365**,  
2848 261–268.

2849 22. Brandt, U. (1999). Control of ubiquinol oxidation at  
2850 center P (Q<sub>o</sub>) of the cytochrome bc<sub>1</sub> complex.  
2851 *J. Bioenerg. Biomembr.* **31**, 243–250.

2852 23. Berry, E. A., Huang, L. S., Zhang, Z. & Kim, S. H.  
2853 (1999). Structure of the avian mitochondrial cyto-  
2854 chrome bc<sub>1</sub> complex. *J. Bioenerg. Biomembr.* **31**,  
2855 177–190.

2856 24. Gao, X., Wen, X., Esser, L., Quinn, B., Yu, L., Yu, C. A.  
2857 & Xia, D. (2003). Structural basis for the quinone  
2858 reduction in the bc<sub>1</sub> complex: a comparative  
2859 analysis of crystal structures of mitochondrial cyto-  
2860 chrome bc<sub>1</sub> with bound substrate and inhibitors at  
2861 the Q(i) site. *Biochemistry*, **42**, 9067–9080.

2862 25. de Vries, S., Albracht, S. P. & Leeuwerik, F. J. (1979).  
2863 The multiplicity and stoichiometry of the prosthetic  
2864 groups in QH<sub>2</sub>: cytochrome c oxidoreductase as  
2865 studied by EPR. *Biochim. Biophys. Acta*, **546**, 316–333.

2866 26. Glaser, E. G., Meinhardt, S. W. & Crofts, A. R. (1984).  
2867 Reduction of cytochrome b-561 through the anti-  
2868 mycin-sensitive site of the ubiquinol-cytochrome c<sub>2</sub>  
2869 oxidoreductase complex of Rhodospseudomonas  
2870 sphaeroides. *FEBS Letters*, **178**, 336–342.

2871 27. Meinhardt, S. & Crofts, A. (1984). In *Advances in*  
2872 *Photosynthesis Research* (Sybesma, C., ed.), vol. 1, pp.  
2873 649–652, Martinus Nijhoff/Dr. W. Junk Publishers,  
2874 The Hague.

2875 28. Robertson, D. E., Prince, R. C., Bowyer, J. R.,  
2876 Matsuura, K., Dutton, P. L. & Ohnishi, T. (1984).  
2877 Thermodynamic properties of the semiquinone and  
2878 its binding site in the ubiquinol-cytochrome c (c<sub>2</sub>)  
2879 oxidoreductase of respiratory and photosynthetic  
2880 systems. *J. Biol. Chem.* **259**, 1758–1763.

2881 29. Salerno, J. C., Xu, Y., Osgood, M. P., Kim, C. H. & King,  
2882 T. E. (1989). Thermodynamic and spectroscopic  
2883 characteristics of the cytochrome bc<sub>1</sub> complex. Role  
2884 of quinone in the behavior of cytochrome b<sub>562</sub>. *J. Biol.*  
2885 *Chem.* **264**, 15398–15403.

2886 30. Rich, P. R., Jeal, A. E., Madgwick, S. A. & Moody, A. J.  
2887 (1990). Inhibitor effects on redox-linked protonations  
2888 of the b haems of the mitochondrial bc<sub>1</sub> complex.  
2889 *Biochim. Biophys. Acta*, **1018**, 29–40.

2890 31. Crofts, A., Barquera, B., Bechmann, G., Guergova, M.,  
2891 Salcedo-Hernandez, R., Hacker, B. *et al.* (1995). In  
2892 *Photosynthesis: From Light to Biosphere* (Mathis, P., ed.),  
2893 Vol. II, pp. 493–500, Kluwer Academic, Dordrecht.

2894 32. Kunz, W. S. & Konstantinov, A. A. (1983). Effect of  
2895 b-c<sub>1</sub>-site inhibitors on the midpoint potentials of  
2896 mitochondrial cytochromes b. *FEBS Letters*, **155**,  
2897 237–240.

2898 33. Dikanov, S. A., Samoilova, R. I., Kolling, D. R.,  
2899 Holland, J. T. & Crofts, A. R. (2004). Hydrogen  
2900 bonds involved in binding the Q<sub>i</sub>-site semiquinone  
2901 in the bc<sub>1</sub> complex, identified through deuterium  
2902 exchange using pulsed EPR. *J. Biol. Chem.* **279**,  
2903 15814–15823.

2904 34. Mitani, S., Araki, S., Takii, Y., Ohshima, T., Matsuo, N.  
2905 & Miyoshi, H. (2001). The biochemical mode of action  
2906 of the novel selective fungicide cyazofamid: specific  
2907 inhibition of mitochondrial complex III in *Phythyum*  
2908 *spinosum*. *Pesticide Biochem. Physiol.* **71**, 107–115(9).

2899 35. Ohshima, T. & Komyoji, T. (2004). Development of a  
2900 a novel fungicide, cyazofamid. Mitani, S.; Matsuo, N.;  
2901 Nakajima, T. *J. Pestic. Sci.*, **29**, 136–138.

2902 36. Dickie, J. P., Loomans, M. E., Farley, T. M. & Strong,  
2903 F. M. (1963). The chemistry of antimycin A. Xi.  
2904 3-substituted 3-formamidosalicylic amides. *J. Med.*  
2905 *Chem.* **122**, 424–427.

2906 37. Miyoshi, H., Kondo, H., Oritani, T., Saitoh, I. &  
2907 Iwamura, H. (1991). Inhibition of electron transport of  
2908 rat liver mitochondria by unnatural (-)-antimycin A3.  
2909 *FEBS Letters*, **292**, 61–63.

2910 38. Miyoshi, H., Tokutake, N., Imaeda, Y., Akagi, T. &  
2911 Iwamura, H. (1995). A model of antimycin A binding  
2912 based on structure-activity studies of synthetic  
2913 antimycin A analogues. *Biochim. Biophys. Acta*, **1229**,  
2914 149–154.

2915 39. Tokutake, N., Miyoshi, H., Nakazato, H. & Iwamura,  
2916 H. (1993). Inhibition of electron transport of rat-liver  
2917 mitochondria by synthesized antimycin A analogs.  
2918 *Biochim. Biophys. Acta*, **1142**, 262–268.

2919 40. Tokutake, N., Miyoshi, H., Satoh, T., Hatano, T. &  
2920 Iwamura, H. (1994). Structural factors of antimycin A  
2921 molecule required for inhibitory action. *Biochim.*  
2922 *Biophys. Acta*, **1185**, 271–278.

2923 41. Neft, N. & Farley, T. M. (1971). Inhibition of electron  
2924 transport by substituted salicyl-N-(n-octadecyl)  
2925 amides. *J. Med. Chem.* **14**, 1169–1170.

2926 42. Kim, H., Esser, L., Hossain, M. B., Xia, D., Yu, C.-A.,  
2927 Rizo, J. *et al.* (1999). Structure of antimycin A1, a  
2928 specific electron transfer inhibitor of ubiquinol-  
2929 cytochrome c oxidoreductase. *J. Am. Chem. Soc.* **121**,  
2930 4902–4903.

2931 43. Birch (1961). *J. Chem. Soc.*, 889.

2932 44. van Tamelan, E. E., Dickie, J. P., Loomans, M. E.,  
2933 Dewey, R. S. & Strong, F. M. (1961). *J. Am. Chem. Soc.*  
2934 **83**, 1639–1646.

2935 45. Ha, S. T., Wilkins, C. L. & Abidi, S. L. (1989). Analysis  
2936 of antimycin A by reversed-phase liquid chromatography/  
2937 nuclear magnetic resonance spectrometry. *Anal. Chem.* **61**,  
2938 404–408.

2939 46. Xia, D., Yu, C. A., Kim, H., Xia, J. Z., Kachurin, A. M.,  
2940 Zhang, L. *et al.* (1997). Crystal structure of the  
2941 cytochrome bc<sub>1</sub> complex from bovine heart mitochondria  
2942 [published erratum appears in *Science* 1997  
2943 Dec 19;278(5346):2037]. *Science*, **277**, 60–66.

2944 47. Weiss, M. S. (2001). Global indicators of X-ray data  
2945 quality. *J. Appl. Crystallog.* **34**, 130–135.

2946 48. Vaguine, A. A., Richelle, J. & Wodak, S. J. (1999).  
2947 SFCHECK: a unified set of procedures for evaluating  
2948 the quality of macromolecular structure-factor data  
2949 and their agreement with the atomic model. *Acta*  
2950 *Crystallog. sect. D. Biol. Crystallog.* **55**, 191–205.

2951 49. Collaborative Computational Project, Number 4.  
2952 (1994). The CCP4 suite: programs for protein  
2953 crystallography. *Acta Crystallog. sect. D*, **50**, 760–763.

2954 50. Laskowski, R. A., MacArthur, M. W., Moss, D. S. &  
2955 Thornton, J. M. (1993). *J. Appl. Crystallog.* **26**, 283.

2956 51. Iwata, S., Lee, J. W., Okada, K., Lee, J. K., Iwata, M.,  
2957 Rasmussen, B. *et al.* (1998). Complete structure of the  
2958 11-subunit bovine mitochondrial cytochrome bc<sub>1</sub>  
2959 complex [see comments]. *Science*, **281**, 64–71.

2960 52. Hunte, C., Koepke, J., Lange, C., Rossmann, T. &  
2961 Michel, H. (2000). Structure at 2.3 Å resolution of the  
2962 cytochrome bc<sub>1</sub> complex from the yeast  
2963 *Saccharomyces cerevisiae* co-crystallized with an anti-  
2964 body Fv fragment. *Struct. Fold. Des.* **8**, 669–684.

2965 53. Silman, H. I., Rieske, J. S., Lipton, S. H. & Baum, H.  
2966 (1967). A new protein component of complex 3 of the  
2967 mitochondrial electron transfer chain. *J. Biol. Chem.*  
2968 **242**, 4867–4875.

2969 54. Schagger, H., Brandt, U., Gencic, S. & von Jagow, G.  
2970 (1995). Ubiquinol-cytochrome-c reductase from  
2971 human and bovine mitochondria. *Methods Enzymol.*  
2972 **260**, 82–96.

2973 55. Enders, D., Geibel, G. & Osborne, S. (2000). Diastereo-  
2974 and enantioselective total synthesis of stigmatellin A.  
2975 *Chemistry*, **6**, 1302–1309.

2976 56. Iwata, M. (2001). Structural Studies on cytochrome  
2977 bc<sub>1</sub> complex from Bovine Heart Mitochondria,  
2978 Uppsala University.

2979 57. Berry, E. A. & Huang, L. S. (2003). Observations  
2980 concerning the quinol oxidation site of the cyto-  
2981 chrome bc<sub>1</sub> complex. *FEBS Letters*, **555**, 13–20.

2982 58. Saraste, M. (1984). Location of haem-binding sites in  
2983 the mitochondrial cytochrome b. *FEBS Letters*, **166**,  
2984 367–372.

2985 59. Widger, W. R., Cramer, W. A., Herrmann, R. G. &  
2986 Trebst, A. (1984). Sequence homology and structural  
2987 similarity between cytochrome b of mitochondrial  
2988 complex III and the chloroplast b6-f complex: position  
2989 of the cytochrome b hemes in the membrane. *Proc.*  
2990 *Natl Acad. Sci. USA*, **81**, 674–678.

2991 60. Crofts, A., Robinson, H., Andrews, K., van Doren, S. &  
2992 Berry, E. (1988). Catalytic sites for reduction and  
2993 oxidation of quinones. In *Cytochrome Systems* (Papa,  
2994 S., ed.), pp. 617–624, Plenum Press, New York.

2995 61. Berry, E. A., Zhang, Z., Huang, L. S. & Kim, S. H.  
2996 (1999). Structures of quinone binding sites in bc  
2997 complexes: functional implications. *Biochem. Soc.*  
2998 *Trans.* **27**, 565–572.

2999 62. Gray, K. A., Dutton, P. L. & Daldal, F. (1994).  
3000 Requirement of histidine 217 for ubiquinone  
3001 reductase activity (Qi site) in the cytochrome bc<sub>1</sub>  
3002 complex. *Biochemistry*, **33**, 723–733.

3003 63. Xu, J. X., Xiao, Y., Wang, Y. H., Li, X. & Gu, L. Q. (1993).  
3004 Comparison between the properties of 3-nitrosalicyl-  
3005 N-alkylamide and antimycin A acting on QH<sub>2</sub>:cyto-  
3006 chrome c reductase. *Biochim. Biophys. Acta*, **1142**,  
3007 83–87.

3008 64. Lange, C. & Hunte, C. (2002). Crystal structure of the  
3009 yeast cytochrome bc<sub>1</sub> complex with its bound  
3010 substrate cytochrome c. *Proc. Natl Acad. Sci. USA*, **99**,  
3011 2800–2805.

3012 65. Hunte, C., Solmaz, S. & Lange, C. (2002). Electron  
3013 transfer between yeast cytochrome bc<sub>1</sub> complex and  
3014 cytochrome c: a structural analysis. *Biochim. Biophys.*  
3015 *Acta*, **1555**, 21–28.

3016 66. Gao, X., Wen, X., Yu, C., Esser, L., Tsao, S., Quinn, B.  
3017 *et al.* (2002). The crystal structure of mitochondrial  
3018 cytochrome bc<sub>1</sub> in complex with famoxadone: the role  
3019 of aromatic-aromatic interaction in inhibition.  
3020 *Biochemistry*, **41**, 11692–11702.

3021 67. Lovell, S. C., Word, J. M., Richardson, J. S. &  
3022 Richardson, D. C. (2000). The penultimate rotamer  
3023 library. *Proteins: Struct. Funct. Genet.* **40**, 389–408.

3024 68. Schnauffer, A., Sbicego, S. & Blum, B. (2000).  
3025 Antimycin A resistance in a mutant *Leishmania*  
3026 tarentolae strain is correlated to a point mutation in  
3027 the mitochondrial apocytochrome b gene. *Curr. Genet.*  
3028 **37**, 234–241.

3029 69. Lowry, O. H., Rosebrough, N. J., Farr, A. L. & Randall,  
3030 R. J. (1951). Protein measurement with the Folin  
3031 phenol reagent. *J. Biol. Chem.* **193**, 265–275.

3032 70. Berry, E. A., Huang, L. S. & DeRose, V. J. (1991).  
3033 Ubiquinol-cytochrome c oxidoreductase of higher  
3034

3025 plants. Isolation and characterization of the bc<sub>1</sub>  
 3026 complex from potato tuber mitochondria. *J. Biol.*  
 3027 *Chem.* **266**, 9064–9077.  
 3028 71. Otwinowski, Z. & Minor, W. (1997). Processing of  
 3029 X-ray Diffraction Data Collected in Oscillation Mode.  
 3030 In *Macromolecular Crystallography, part A* (Carter,  
 3031 C. W. J. & Sweet, R. M., eds), vol. 276, pp. 307–326,  
 3032 Academic Press, New York.  
 3033 72. Brunger, A. T. (1992). The free R value: a novel  
 3034 statistical quantity for assessing the accuracy of  
 3035 crystal structures. *Nature*, **355**, 472–474.  
 3036 73. Jones, T. A., Zhou, J.-Y., Cowan, S. W. & Kjeldgaard,  
 3037 M. (1991). Improved methods for building protein  
 3038 models in electron density maps and the location of  
 3039 errors on these models. *Acta Crystallog. sect. A*, **47**,  
 3040 110–119.  
 3041 74. Brunger, A. T., Adams, P. D., Clore, G. M., DeLano,  
 3042 W. L., Gros, P., Grosse-Kunstleve, R. W. *et al.* (1998).  
 3043 Crystallography and NMR system: a new software  
 3044 suite for macromolecular structure determination.  
 3045 *Acta Crystallog. sect. D Biol. Crystallog.* **54**, 905–921.  
 3046 75. Hoof, R. W., Vriend, G., Sander, C. & Abola, E. E.  
 3047 (1996). Errors in protein structures. *Nature*, **381**, 272.  
 3048 76. Perrakis, A., Harkiolaki, M., Wilson, K. S. & Lamzin,  
 3049 V. S. (2001). ARP/wARP and molecular replacement.  
 3050 *Acta Crystallog. sect. D Biol. Crystallog.* **57**, 1445–1450.  
 3051 77. Berry, E. A., Huang, L.-S., Saechao, L. K., Pon, N. G.,  
 3052 Valkova-Valchanova, M. & Daldal, F. (2004). X-ray  
 3053 structure of *Rhodobacter capsulatus* cytochrome bc<sub>1</sub>:  
 3054 comparison with its mitochondrial and chloroplast  
 3055 counterparts. *Photosynth. Res.* **81**, 251–275.

*Edited by R. Huber*

(Received 28 February 2005; received in revised form 10 May 2005; accepted 19 May 2005)